

# Strong coupling electron-photon dynamics: a real-time investigation of energy redistribution in molecular polaritons

Matteo Castagnola,<sup>†</sup> Marcus T. Lexander,<sup>†</sup> Enrico Ronca,<sup>\*,‡</sup> and Henrik Koch<sup>\*,†</sup>

<sup>†</sup>*Department of Chemistry, Norwegian University of Science and Technology, 7491 Trondheim, Norway*

<sup>‡</sup>*Dipartimento di Chimica, Biologia e Biotecnologie, Università degli Studi di Perugia, Via Elce di Sotto, 8, 06123, Perugia, Italy*

E-mail: enrico.ronca@unipg.it; henrik.koch@ntnu.no

## Abstract

We analyze the real-time electron-photon dynamics in long-range polariton-mediated energy transfer using a real-time quantum electrodynamics coupled cluster (RT-QED-CC) model, which allows for spatial and temporal visualization of transport processes. We compute the time evolution of photonic and molecular observables, such as the dipole moment and the photon coordinate, following the excitation of the system induced by short laser pulses. Our simulation highlights the different time scales of electrons and photons under light-matter strong coupling, the role of dark states, and the differences with the electronic (Förster and Dexter) energy exchange mechanisms. The developed method can simulate multiple high-intensity laser pulses while explicitly retaining electronic and electron-photon correlation and is thus suited for nonlinear optics and transient absorption spectroscopies of molecular polaritons.

## Introduction

When a molecular excitation strongly interacts with a confined optical mode (e.g., in a Fabry-Pérot cavity), hybrid light-matter states, called polaritons, are formed. Polaritons have

recently attracted interest from chemists due to pioneering experiments proving modifications in chemical properties, such as photochemistry and ground state reactivity.<sup>1-9</sup> Several works suggest a modified electronic dynamics under light-matter strong coupling, showing e.g. changes in lifetimes,<sup>1,10</sup> selection rules in multi-photon absorption,<sup>11</sup> energy transfer,<sup>12-18</sup> as well as enhanced nonlinear optical properties.<sup>19-23</sup> The proper understanding of such experimental findings in cavity-modified chemistry thus requires a microscopic model of the electron-photon interplay.

In this paper, we take another step forward in describing polaritons by explicitly modeling laser-driven molecules in quantum cavities via real-time quantum electrodynamics coupled cluster (RT-QED-CC). The *ab initio* QED-CC parametrization of the polaritonic wave function, which includes electron-electron and electron-photon correlation,<sup>24,25</sup> provides a nonperturbative description of the electron-photon dynamics. We can hence reliably describe both the long-range photonic correlation and the short-range intra- and intermolecular electronic forces. The temporal evolution of the system can be monitored through matter and photon quantities such as the electronic density and the photon number. The RT-QED-CC method is therefore suited for

studying the interaction of molecules and aggregates with confined optical modes from the weak to the ultrastrong coupling regime, even under external high-intensity and ultrashort electric pulses (linear and nonlinear excitation regimes). Our method can support the study of quantum light spectroscopies,<sup>26–32</sup> high-order harmonic generation,<sup>19–21</sup> multi-photon and transient (pump-probe) spectroscopy of molecular polaritons.<sup>10,11,33,34</sup> We here focus on photon-mediated energy transfer as a clear example of experimentally investigated electron-photon dynamics<sup>12–16</sup> with potential applications in light-harvesting systems.

Our method allows spatial and temporal visualization of the transport process, following the real-time quantum coherent oscillations in the molecular density and observables such as the dipole moment. Moreover, since we explicitly include the QED field, we describe in real-time the role of the optic environment and its entanglement with matter, computing photon quantities such as the photon coordinate. Our results highlight different time scales in the electron-photon dynamics, the role of the dark states, and the modified interaction of polaritons with external pulses. Moreover, RT-QED-CC can also accurately model the short-range electronic energy transfer (Förster and Dexter), offering a clear discussion of the similarities and differences with the photonic channel. While our method is so far designed for electronic strong coupling (ESC), we believe the concepts we developed for polaritonic energy redistribution can also be applied to vibrational strong coupling (VSC).<sup>18,35–37</sup>

The paper is organized as follows. First, we briefly introduce the theory behind *ab initio* quantum electrodynamics (QED) and describe the QED Hartree-Fock (QED-HF) and QED-CC methods. Next, we provide a detailed description of the real-time QED-CC wave function and discuss the novel information we can extract by explicitly modeling the photonic degrees of freedom. We then apply the RT-QED-CC method to study energy transfers in molecular polaritons. Finally, we summarize the main results presented in the paper and discuss fu-

ture perspectives and applications of the developed framework.

## *Ab initio* coupled cluster for molecular polaritons

In this section, we introduce the QED-HF and QED-CC methods and focus on the real-time description of the QED-CC parametrization. The photons are described at the same level as the electrons in a polaritonic wave function. To this end, we employ the non-relativistic Pauli-Fierz Hamiltonian in the dipole approximation, Born-Oppenheimer approximation, and length representation,<sup>38,39</sup> here expressed in second quantization and atomic units

$$\begin{aligned}
 H = & \sum_{pq} h_{pq} E_{pq} + \frac{1}{2} \sum_{pqrs} g_{pqrs} e_{pqrs} + h_{nuc} \\
 & + \sqrt{\frac{\omega}{2}} (\boldsymbol{\lambda} \cdot \mathbf{d})_{pq} E_{pq} (b^\dagger + b) \\
 & + \frac{1}{2} \sum_{pqrs} (\boldsymbol{\lambda} \cdot \mathbf{d})_{pq} (\boldsymbol{\lambda} \cdot \mathbf{d})_{rs} E_{pq} E_{rs} \\
 & + \omega b^\dagger b, \tag{1}
 \end{aligned}$$

where  $E_{pq} = \sum_{\sigma} a_{p\sigma}^\dagger a_{q\sigma}$  and  $e_{pqrs} = E_{pq} E_{rs} - \delta_{qr} E_{ps}$  are the spin-adapted singlet electronic operators in second quantization, where the indices  $p, q, r$ , and  $s$  label the one-electron basis.<sup>25</sup> The quantities  $h_{pq}$ ,  $g_{pqrs}$ , and  $\mathbf{d}_{pq}$  are the one-electron, two-electron, and dipole integrals, respectively. The operators  $b^\dagger$  and  $b$  create and annihilate photons of a single effective photon mode of frequency  $\omega$ . Finally,  $\boldsymbol{\lambda}$  is the light-matter coupling strength of the photon field. The Hamiltonian in Eq. 1 is employed for the *ab initio* QED-HF and QED-CC methods,<sup>24</sup> which we briefly describe in the following sections.

### QED-HF

The QED-HF wave function is the direct product of a Slater determinant and a photonic state

$$|\mathbf{R}\rangle = |\text{HF}\rangle \otimes \sum_n (b^\dagger)^n |0\rangle c_n, \tag{2}$$

where the optimal parameters are obtained from the variational principle by minimizing the expectation value of the Hamiltonian in Eq. 1.<sup>24</sup> The orbitals are obtained by diagonalization of the QED-HF Fock matrix, while the photon state is a coherent state determined by the molecular dipole moment<sup>24</sup>

$$|R\rangle = |\text{HF}\rangle \otimes U_{\text{QED-HF}} |0\rangle \equiv U_{\text{QED-HF}} |\text{HF}, 0\rangle, \quad (3)$$

where

$$U_{\text{QED-HF}} = \exp\left(-\frac{\boldsymbol{\lambda} \cdot \langle \mathbf{d} \rangle_{\text{QED-HF}}}{\sqrt{2\omega}}(b^\dagger - b)\right). \quad (4)$$

## QED-CC

The QED-HF wave function of Eq. 3 provides the reference state of the QED-CC parametrization, and the coherent-state transformation is handled via a picture change of the Hamiltonian.<sup>24,39</sup> The QED-CC wave function is thus defined in the QED-HF coherent-state representation  $\tilde{H} = U_{\text{QED-HF}}^\dagger H U_{\text{QED-HF}}$ , that is, the Hamiltonian used to determine the CC amplitudes is transformed using Eq. 4

$$\begin{aligned} \tilde{H} = & \sum_{pq} h_{pq} E_{pq} + \frac{1}{2} \sum_{pqrs} g_{pqrs} e_{pqrs} + h_{nuc} \\ & + \sqrt{\frac{\omega}{2}} (\boldsymbol{\lambda} \cdot (\mathbf{d} - \langle \mathbf{d} \rangle_{\text{QED-HF}})) (b^\dagger + b) \\ & + \frac{1}{2} (\boldsymbol{\lambda} \cdot (\mathbf{d} - \langle \mathbf{d} \rangle_{\text{QED-HF}}))^2 \\ & + \omega b^\dagger b. \end{aligned} \quad (5)$$

As for the electronic coupled cluster,<sup>25</sup> the QED-CC wave function is given by an exponential parametrization

$$|\text{QED-CC}\rangle = e^T |\text{HF}, 0\rangle, \quad (6)$$

where the cluster operator  $T$  includes electronic, photonic, and electron-photon excitations.<sup>24</sup> In this paper, we use the QED-CCSD-1 model,<sup>24</sup> which includes single and double excitations in the electronic space and a single

excitation for the photon

$$T = T_e + T_{int} + T_p, \quad (7)$$

where

$$T_e = \sum_{ai} t_{ai} E_{ai} + \frac{1}{2} \sum_{aibj} t_{aibj} E_{ai} E_{bj} \quad (8)$$

$$T_{int} = \sum_{ai} s_{ai} E_{ai} b^\dagger + \frac{1}{2} \sum_{aibj} s_{aibj} E_{ai} E_{bj} b^\dagger \quad (9)$$

$$T_p = \gamma b^\dagger. \quad (10)$$

In these equations,  $i$  and  $j$  label occupied orbitals, and  $a$  and  $b$  label virtual orbitals of the QED-HF reference determinant. The QED-CC amplitudes are then obtained by projection of the Schrödinger equation. In the same way, the QED-CC dual state is defined as

$$\langle \Lambda | = \langle \text{HF}, 0 | + \sum_{\mu, n} \bar{t}_{\mu n} \langle \mu, n | e^{-T}, \quad (11)$$

where  $\bar{t}_{\mu n}$  are the Lagrangian multipliers for the  $|\mu, n\rangle$  excitation.<sup>24,25</sup>

The QED-CC parametrization allows for a flexible description of the ground state, including both electron-electron and electron-photon correlation. Following the same approach as for electronic CC, we can then obtain information on the molecular-polariton excited states using the equation of motion (EOM) or response formalism.<sup>24,25,39-41</sup> These effectively time-independent approaches rely upon the Fourier transformation of any perturbation applied to the system. In the following, we describe a different approach based on a real-time propagation of the CC amplitudes.

## Real-time QED-CC

We aim to study the time evolution of the electron-photon system subject to an external field  $V(t)$  such as an electric pump. The total Hamiltonian is thus  $\tilde{H} + \tilde{V}(t)$  (in the QED-HF coherent state representation of Eq. 5), and we parametrize the time-evolution using time-dependent amplitudes  $T(t)$  and a complex global-phase parameter  $\alpha(t)$ , similarly to elec-

$$|\text{QED-CC}\rangle(t) = e^{T(t)} |\text{HF}, 0\rangle e^{i\alpha(t)}. \quad (12)$$

The amplitudes are obtained by projection of the time-dependent Schrödinger equation<sup>40,41,48</sup>

$$\frac{d\alpha}{dt} = -\langle \text{HF}, 0 | (\tilde{H} + \tilde{V}(t)) e^{T(t)} | \text{HF}, 0 \rangle \quad (13)$$

$$\frac{dt_\mu}{dt} = -i \langle \mu, 0 | e^{-T(t)} (\tilde{H} + \tilde{V}(t)) e^{T(t)} | \text{HF}, 0 \rangle \quad (14)$$

$$\frac{d\gamma}{dt} = -i \langle \text{HF}, n | e^{-T(t)} (\tilde{H} + \tilde{V}(t)) e^{T(t)} | \text{HF}, 0 \rangle \quad (15)$$

$$\frac{ds_\mu}{dt} = -i \langle \mu, n | e^{-T(t)} (\tilde{H} + \tilde{V}(t)) e^{T(t)} | \text{HF}, 0 \rangle, \quad (16)$$

and analogous equations hold for the QED-CC dual state (further details are provided in the Supporting Information).

While response theory would rely on a perturbative expansion to obtain linear and nonlinear response functions in the frequency domain,<sup>39-41</sup> we numerically propagate the amplitudes and multipliers in time. We thus study the electron-photon dynamics computing the mean values of observables  $\langle A \rangle$  at each time step

$$\langle A \rangle(t) = \langle \Lambda(t) | A | \text{QED-CC}(t) \rangle. \quad (17)$$

The information in the frequency domain can then be obtained via a Fourier transform of Eq. 17. Notice that in QED, we have access to additional observables from the explicit modeling of the photon field. We can thus describe photon quantities such as the photon coordinate  $q = \frac{b+b^\dagger}{\sqrt{2\omega}}$ , which is connected to the electric field of the photons in the cavity, or the photon number  $N_{ph} = b^\dagger b$ . We must then account for the picture change of the QED-HF coherent state transformation in Eq. 4 since the QED-CC wave function is defined for the Hamiltonian in Eq. 5.<sup>39</sup>

The RT-QED-CC approach allows for the description of the electron-photon dynamics under ultrashort and intense *classical* electric

fields

$$V(t) = \mathbf{d} \cdot \mathbf{E}_{ext}(t) = \mathbf{d} \cdot \mathcal{E}_0(t) \cos(\omega_{ext}t + \varphi), \quad (18)$$

where  $\mathcal{E}_0(t)$  is an envelope function that describes the shape of the external pulse, and the field-molecule interaction is in the length gauge and dipole approximation. Moreover, the explicit modeling of the photon field provides additional flexibility in the operator  $V(t)$ . We can, in principle, study the dynamics of the electrons interacting with *quantum* light, for instance, a coherent state, by changing the parameters in the transformation Eq. 4. The interaction of molecules with a photon number state can be modeled by setting the appropriate initial state conditions for the QED-CC states. Moreover, while standard molecular spectroscopy focuses on the molecular degrees of freedom, in a QED framework, we can also study the effect of perturbations that couple directly to the photon field (for instance, via external currents), such as

$$V(t) = \mathcal{A}_0(b + b^\dagger) \quad (19)$$

$$V(t) = i\mathcal{B}_0(b - b^\dagger), \quad (20)$$

and subsequently follow the evolution of molecular observables.

The RT-QED-CC method thus allows for a nonperturbative coherent and correlated time-dependent description of the interaction of photons and molecules, permitting the modeling of transient spectroscopies for molecular polaritons, quantum light spectroscopies, molecules in laser fields, and electron-photon quantum entanglement.<sup>10,11,26,28,31,32,49</sup>

## Results and discussions

In this section, the RT-QED-CCSD-1 method is employed to study photon-mediated energy transfers. The RT-QED-CCSD-1 equations have been implemented in a private branch of the  $e^{\mathcal{T}}$  program,<sup>50</sup> and the computational and implementation details are provided in the Supporting Information.

## Intermolecular energy transfer

Electronic intermolecular energy transfer has been experimentally investigated<sup>12-16</sup> due to its potential applications in technologies for e.g. solar cells and light-harvesting systems. While theoretical models were so far limited to simplified methods,<sup>17</sup> we here provide an *ab initio* QED-CC simulation in real-time, with microscopic spatial and temporal visualization and a correlated description of electronic and photonic quantities.

As a simple system to study the long-range polaritonic energy transfer, we consider two identical but perpendicular H<sub>2</sub> molecules in the xy-plane, with the cavity field tuned to their first bright molecular excitation (see Fig. 1). The light-matter coupling strength is here set to 0.01 a.u. with polarization  $\epsilon = (1/\sqrt{2}, 1/\sqrt{2}, 0)$ , such that both the H<sub>2</sub> are coupled to the optical environment. The intermolecular distance is large enough to suppress any electronic coupling between them ( $D = 50 \text{ \AA}$ ). Further computational details are provided in the Supporting Information. In Fig. 1, we show selected snapshots of the differential electronic density (compared to the ground state) in the xy-plane following the interaction with an ultrashort classical electric pulse (see Eq. 18) centered at  $t = 20 \text{ a.u.}$  and polarized along the x-direction (parallel to one of the H<sub>2</sub>).<sup>1</sup> While the electric field polarizes both molecules (see the second panel of Fig. 1), only one of them is excited after the pulse has passed because of their orientation. In the absence of the photon coupling, the electron density of the excited molecule oscillates in time while nothing would happen to the second H<sub>2</sub>. However, when the system is coherently coupled to an optical environment such as a Fabry-Pérot cavity, the excited molecule can transfer energy to the photon field, which, in turn, excites the other H<sub>2</sub> molecule. In Fig. 1, we thus see an ultralong energy transfer mediated by the cavity field. For computational reasons, we used a specific orientation to selectively excite only one H<sub>2</sub>. However, longer

pulses can be used to selectively excite a single species and thus trigger a cavity-mediated energy transfer between different molecules in quantum cavities.<sup>12-16</sup> Notice that since no decoherence is introduced in the simulation, the excitation will be transferred back and forth between the H<sub>2</sub> molecules in a quasi-periodic fashion.

The electron-photon dynamics is more easily analyzed by studying the time-evolution of observables such as the dipole moment  $\mathbf{d}$  and the photon coordinate  $q = (b^\dagger + b)/\sqrt{2\omega}$ . In the upper panel of Fig. 2, we plot the x and y components of the dipole moment for the process pictorially illustrated in Fig. 1. The y component of the dipole moment provides a simple measure of the excitation of the second H<sub>2</sub>. The panel clearly illustrates the fast density fluctuations and the slower energy transfer between the two molecules. The time evolution of the dipole moment for the undressed (out-of-cavity) electron dynamics is reported in the Supporting Information, and it does not show any energy transfer due to the large distance between the molecules. To follow the excitation of the quantum cavity, we report the photon coordinate  $\langle q \rangle = \langle b^\dagger + b \rangle / \sqrt{2\omega}$  in the lower panel of Fig. 2. It is interesting to notice that photon and matter observables show out-of-phase oscillations and seem to display a different time period, with *two* maxima for  $\langle q \rangle$  in a *single* (back and forth) energy transfer between the H<sub>2</sub> molecules. The reason for this (apparent) period difference is that each  $\langle q \rangle$  maximum refers to *one of the* H<sub>2</sub> transferring their excitation to the photon field. This is illustrated more clearly using two slightly different molecules, stretching the bond length of the H<sub>2</sub> along y. The dipole moment components and the photon coordinate for this system are illustrated in Fig. 3. The photon and matter degrees of freedom now exhibit the same characteristic time, but there are still two maxima in the photon coordinate for the back-and-forth energy transfer. However, the two peaks are now different as they refer to molecules *with slightly different excitations* transferring energy to the optical field. From Fig. 3, it is also clear that there are more time scales involved compared to Fig. 2,

<sup>1</sup>Videos of the energy-transfer dynamics are available in the following repository: DOI:10.5281/zenodo.10813660.

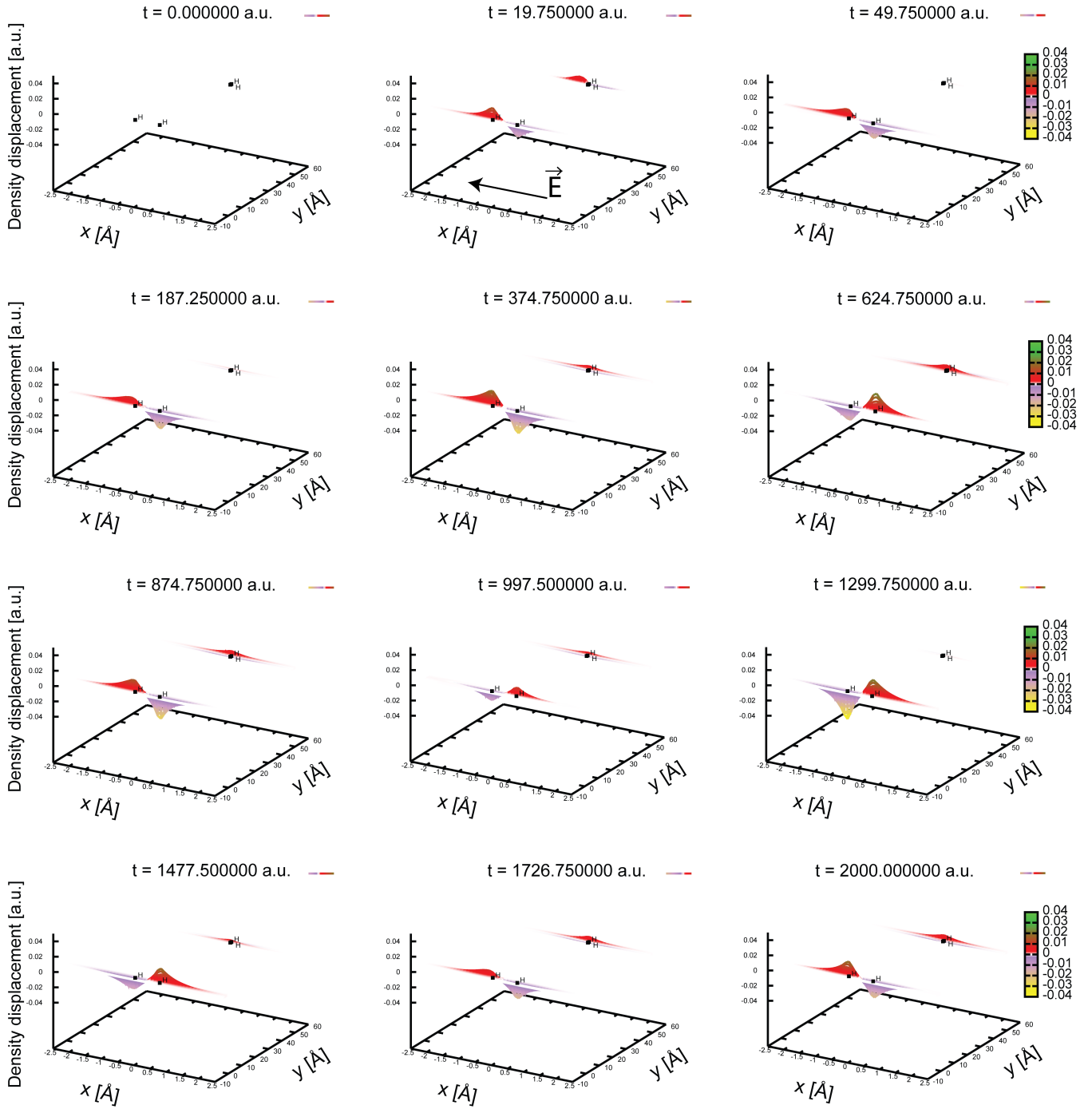


Figure 1: Electron density displacement (compared to the molecular ground state) for two identical but perpendicular  $\text{H}_2$  molecules placed on the  $xy$  plane, at different times. The distance between them is  $D = 50 \text{ \AA}$  and the light-matter coupling strength is  $0.01 \text{ a.u.}$ , with photon polarization oriented such that both molecules are coupled to the cavity  $\epsilon = (1/\sqrt{2}, 1/\sqrt{2}, 0)$ . The molecules are perturbed by an ultrashort classical electric pulse centered at  $20 \text{ a.u.}$  (second panel), but only the  $\text{H}_2$  parallel to the classical electric field is excited after the pulse passes. The density of the excited molecule then oscillates in time. However, in a quantum cavity, the excitation is transferred to the photon field, which in turn excites the other  $\text{H}_2$ , thus allowing for ultralong range energy transfer. As time passes, the second molecule transfers its energy back to the photon field and eventually to the first molecule since no decoherence is present so far in the simulations.

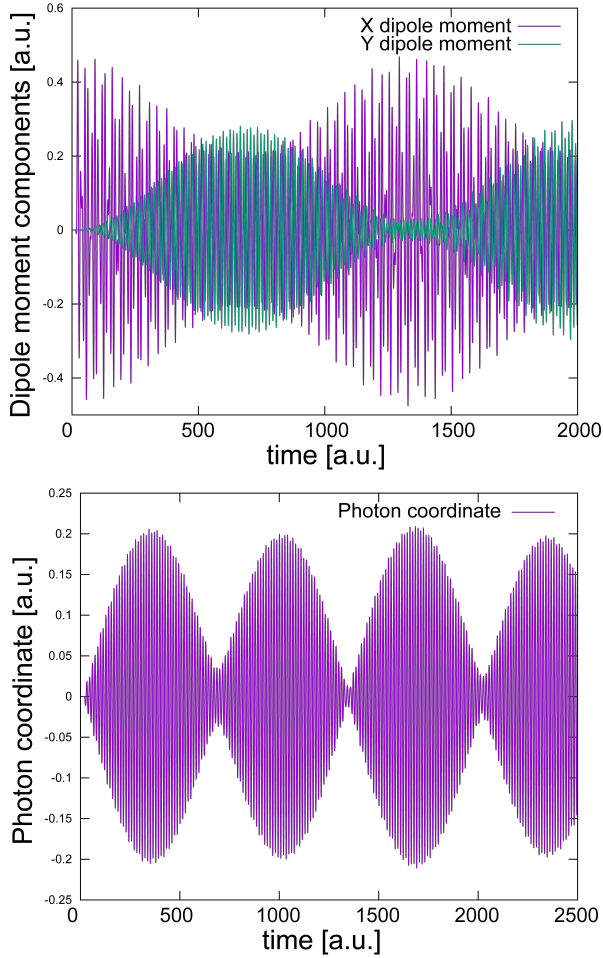


Figure 2: Dipole moment  $\mathbf{d}$  components (upper panel) and photon coordinate  $\frac{\langle b^\dagger + b \rangle}{\sqrt{2\omega}}$  (lower panel) for the dynamics depicted in Fig. 1. The y component of the dipole moment provides a simple measure of the excitation transfer between the  $\text{H}_2$  molecules, while the photon coordinate illustrates the photon excitation inside the cavity.

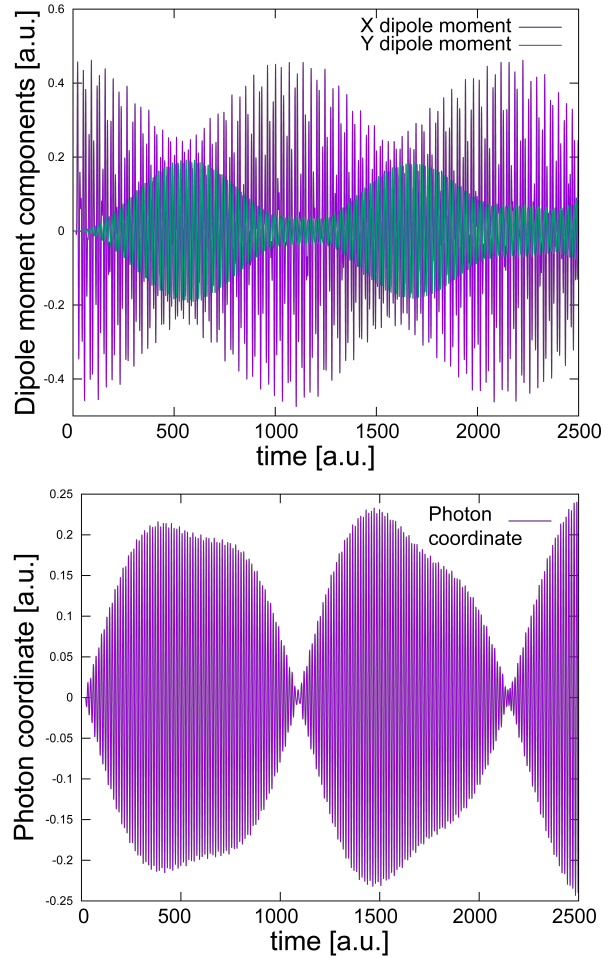


Figure 3: Dipole moment  $\mathbf{d}$  components (upper panel) and photon coordinate  $\frac{\langle b^\dagger + b \rangle}{\sqrt{2\omega}}$  (lower panel) for the dynamics of two slightly different  $\text{H}_2$  molecules (of bond lengths  $0.76 \text{ \AA}$  and  $0.78 \text{ \AA}$ ), with orientation, cavity field, and external pulse as in Fig. 1. The system is thus endowed with three distinct polaritonic states (lower, middle, and upper polaritons). Since the two undressed  $\text{H}_2$  excitations are slightly different, the maxima in the photon coordinate envelope (second panel) are now different, contrary to Fig. 2.

as can also be inferred from a simple Jaynes-Cummings (JC) analysis. In the JC model, the system in Fig. 1 is described as two identical two-level oscillators resonantly coupled to the cavity field. There are then three different eigenstates: the upper  $|\text{UP}\rangle$  and lower  $|\text{LP}\rangle$  polaritons, and one dark state  $|\text{DS}\rangle$  (of the same energy as the  $\text{H}_2$  excited state and the photon)

$$|\text{UP}\rangle = \frac{1}{\sqrt{2}} \left( \frac{|e_1 g_2 0\rangle + |g_1 e_2 0\rangle}{\sqrt{2}} + |g_1 g_2 1\rangle \right) \quad (21)$$

$$|\text{DS}\rangle = \frac{|e_1 g_2 0\rangle - |g_1 e_2 0\rangle}{\sqrt{2}} \quad (22)$$

$$|\text{LP}\rangle = \frac{1}{\sqrt{2}} \left( \frac{|e_1 g_2 0\rangle + |g_1 e_2 0\rangle}{\sqrt{2}} - |g_1 g_2 1\rangle \right), \quad (23)$$

where  $e_p$  ( $g_p$ ) refers to the  $p$ -th  $\text{H}_2$  molecule in the excited (ground) state, and 0 (1) to the zero- (one-) photon states. Notice that the dark state  $|\text{DS}\rangle$ , while showing no contribution from the photon field, has a non-zero transition dipole moment due to the different orientation of the molecules

$$\langle g_1 g_2 0 | \mathbf{d} | \text{DS} \rangle = \left( \langle g_1 | x_1 | e_1 \rangle, -\langle g_2 | y_2 | e_2 \rangle, 0 \right)^T. \quad (24)$$

After the pulse has passed, the system is still mainly in the ground state (linear excitation regime) superimposed with the polaritonic and dark states

$$|e_1 g_2 0\rangle = \frac{1}{2} (|\text{UP}\rangle + |\text{LP}\rangle + \sqrt{2} |\text{DS}\rangle). \quad (25)$$

The interference between the involved states thus generates the modulation of the oscillation amplitude (quantum beats) in Fig. 2. There are indeed three fast time scales, associated with the excitation energies of the polaritonic and dark states, but only two slow time scales given by the Rabi splitting (UP-LP energy splitting) and the LP-DS energy difference. In fact, the LP-DS and UP-DS energy difference is the same, and it is exactly half the Rabi splitting in the JC model. On the other hand, when the hydrogens are different, as in Fig. 3, three *polaritonic* states are formed: the upper (UP), middle (MP), and lower (LP) po-

laritons. In this case, three distinct fast time scales are present (from the MP-LP, MP-UP, and LP-UP energy differences), which explains why the photon revival in Fig. 3 differs from the first oscillation. These simulations also demonstrate how the dark states can actively participate in the electron-photon dynamics of the system in the strong coupling regime.

The cavity photons thus provide a novel pathway for intermolecular energy transfer. Electronic energy transfer in chemistry usually arises from a dipole-dipole (Förster) or electronic-exchange (Dexter) mechanism and both are highly dependent on the distance and orientation of the involved molecules.<sup>51</sup> Since the CC parametrization includes electron correlation, our method can describe intermolecular forces and is thus also suited for interacting molecules. In Fig. 4, we report the energy transfer between two  $\text{H}_2$  molecules with the same parameters as in Fig. 1, but for a shorter intermolecular distance  $D = 5 \text{ \AA}$ . The last panel of Fig. 4 shows the out-of-cavity (no QED) simulation of the x and y dipole moments, which illustrates the energy transfer due to the electronic coupling. Inside the cavity (first two panels), both the electronic and polaritonic mechanisms are clearly involved, as we see the faster sinusoidal polaritonic energy transfer together with the electronic energy transfer. Notice that the photon-mediated energy transfer is faster and more efficient than the electronic mechanism. In Fig. 5, we show the same simulation for two slightly different  $\text{H}_2$  molecules. Due to the different excitation energies, almost no energy transfer occurs without the photon field involvement (last panel), while two distinct photon maxima are highlighted due to the coupling of the different  $\text{H}_2$  molecules to the optical device, as in Fig. 3. Polaritons thus provide an alternative energy-transfer channel subject to different requirements than standard electronic transfer. Dexter energy transfer requires strong electronic couplings and is thus relevant only for very short distances, while the Förster mechanism decays as the sixth power of the intermolecular separation  $1/R^6$ . The Förster energy transfer also requires dipole-allowed molecular transitions and depends on



the relative molecular orientation. In addition, the involved excitations need to have similar energies: the fluorescence spectrum of the energy-donor molecule must have a significant spectral overlap with the absorption spectrum of the acceptor molecule. On the other hand, the polaritonic mechanism is virtually distance-independent, only requiring bright (dipole-allowed) molecular excitations coupled to a quasi-resonant optical device. In this case, the relative molecular orientation is less critical, while both excitations must hybridize by coupling to the same optical mode.

Finally, we investigated how the electron-photon dynamics changes with the light-matter coupling strength  $\lambda$  and the number of identical replicas  $N$  of the system (see also the Supporting Information). Since the time scale of the photon-mediated energy transfer depends on the Rabi splitting, it is inversely proportional to  $\lambda$  and the square root of  $N$ . That is, the time scale depends only on the inverse of the *collective* coupling strength  $\lambda\sqrt{N}$ , which means that such processes are relevant in the thermodynamic limit  $N \rightarrow \infty$ ,  $\lambda\sqrt{N} = \text{const.}$  and the time scales can be reduced by simply increasing the molecular concentration in the optical device. This is shown in the Supporting Information for the systems of Fig. 2 and 3 (identical and different  $\text{H}_2$  molecules). At the same time, the energy absorbed and the dipole moment oscillation amplitudes scale linearly when increasing the number of replicas  $N$  subject to *the same* external pulse. This is physically reasonable, and it is correctly modeled via the size intensivity and extensivity of the CC parametrization for the electrons.<sup>25,52</sup> On the other hand, the oscillation amplitudes of the photon coordinate scales as  $\sqrt{N}$ . The amplitude of matter and photon observables thus scale differently with  $N$ , while both are fundamentally independent on  $\lambda$ . These results, therefore, suggest that a relevant amount of energy is stored in the increasing number of dark states.

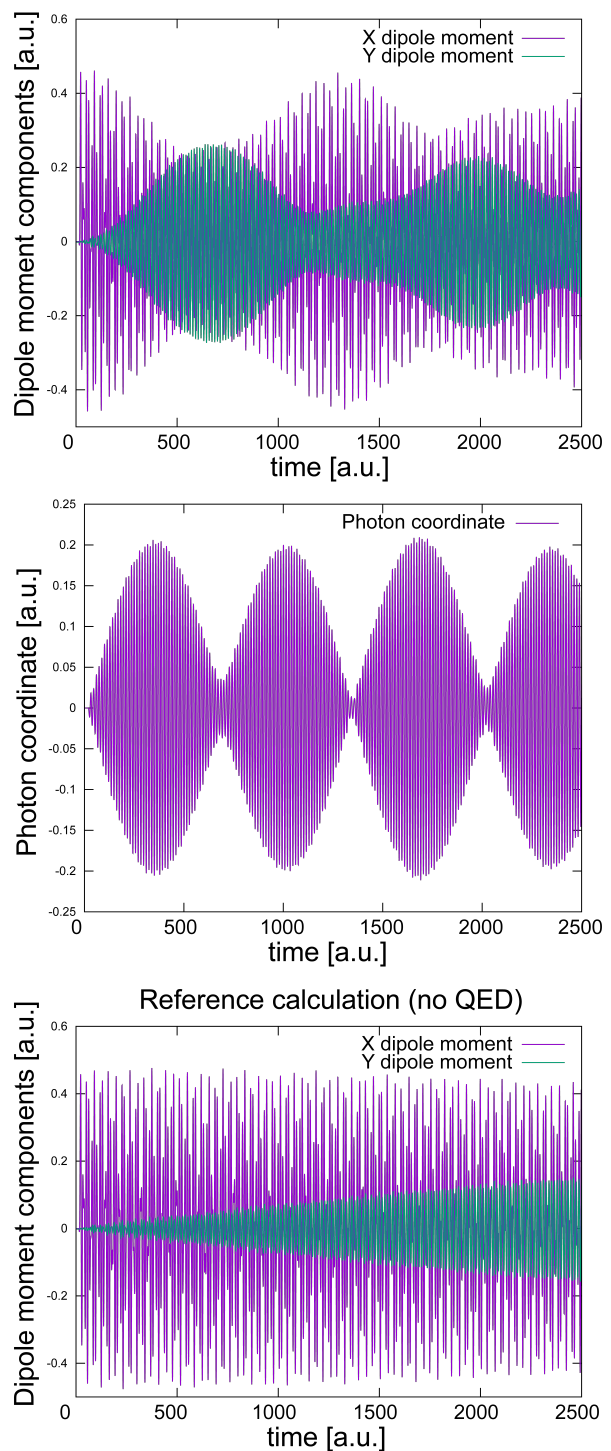


Figure 4: Dipole moment  $\mathbf{d}$  components (upper panel), photon coordinate  $\frac{(b^\dagger + b)}{\sqrt{2\omega}}$  (middle panel), and reference dipole moment simulation (no QED, lower panel) for the dynamics of two perpendicular but identical  $\text{H}_2$  molecules at a distance of  $5 \text{ \AA}$ . Due to electronic coupling, there is an energy transfer even in the absence of the photon field mediation.

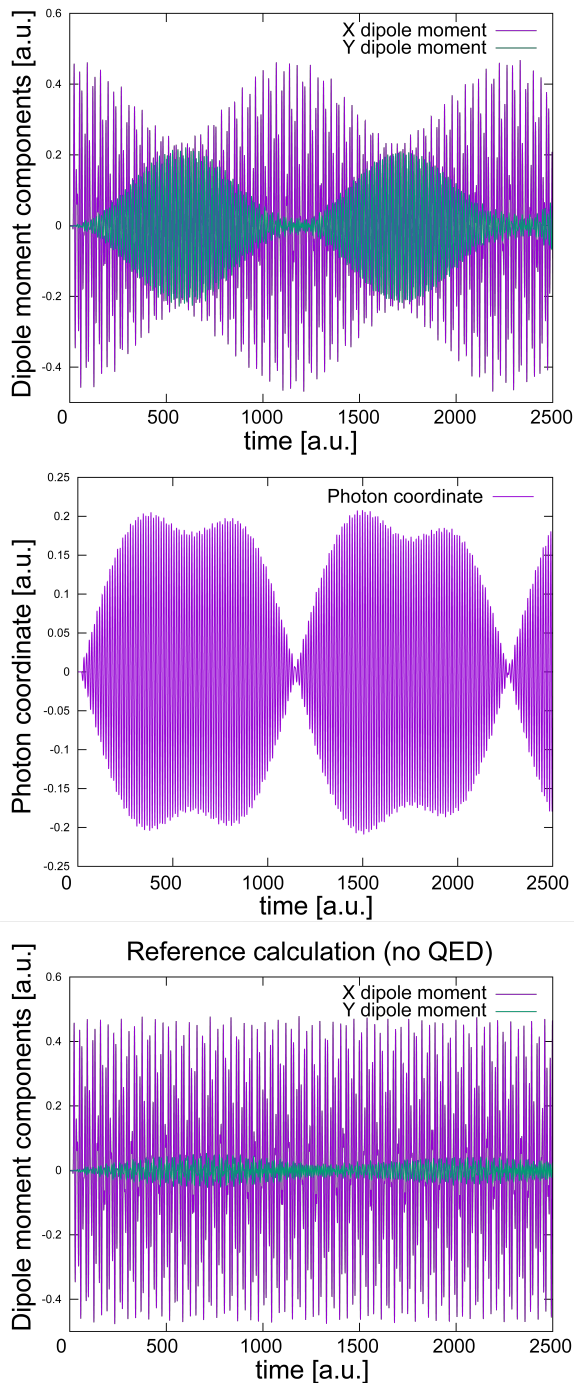


Figure 5: Dipole moment  $\mathbf{d}$  components (upper panel), photon coordinate  $\frac{\langle b^\dagger + b \rangle}{\sqrt{2\omega}}$  (middle panel), and reference dipole moment simulation (no QED, lower panel) for the dynamics of two perpendicular  $\text{H}_2$  molecules with a slightly different bond length at a distance of  $5 \text{ \AA}$ . The electronic coupling is highly dependent on the excitation energy, the orientation, and the distance between the molecules and, compared to Fig. 4, little energy exchange occurs without the photon mediation.

## Photon generation and modified electron-photon dynamics *via* classical pulse sequences

We now focus on the energy transfer and electron-photon dynamics induced by multiple classical electric pulses. In Fig. 6, we report the time evolution of the dipole moment and photon coordinate induced by two short classical electric pulses centered at 20 a.u. and 550 a.u. for the same system depicted in Fig. 1. The second pulse is switched on just before the maximum transfer between the two  $\text{H}_2$  molecules, and the undressed (out-of-cavity) electronic dynamics is reported in the last panel for reference. Notice that no energy transfer occurs outside the cavity because of the large separation between the molecules, as can be inferred from the absence of the y component of the dipole moment in the lowest panel. The  $\text{H}_2$  oriented along the external electric field (x-axis) is excited again by the second pulse, causing a sharp change of the x component of the dipole moment. At the same time, the photon coordinate varies smoothly, but its envelope is modified compared to Fig. 2. Without the second pulse, the photon coordinate amplitude would decrease almost to zero, as shown in Fig. 2. After the  $\text{H}_2$  along x is excited by the second pulse, the photon coordinate increases again, and its envelope amplitude never decreases to zero. This means that, through classical electric fields and their coupling *only to matter*, we generated photons in the optical device that the molecules will not completely absorb as in the vacuum Rabi oscillations of Fig. 2.

Another interesting point of the dynamics in Fig. 2 is the photon coordinate maximum, which occurs before the energy transfer between the  $\text{H}_2$  is complete. In Fig. 7, we show the dynamics of the system under the influence of two pulses centered at 20 a.u. and 300 a.u.. The central time of the second pulse now roughly corresponds to the first maximum of  $\langle q \rangle$  in Fig. 2. In Tab. 1, we report the energy of the system (inside and outside the cavity) before and after each pulse. It is interesting that the optical device changes the interaction of the second pulse with the molecules. In the reference (no QED)

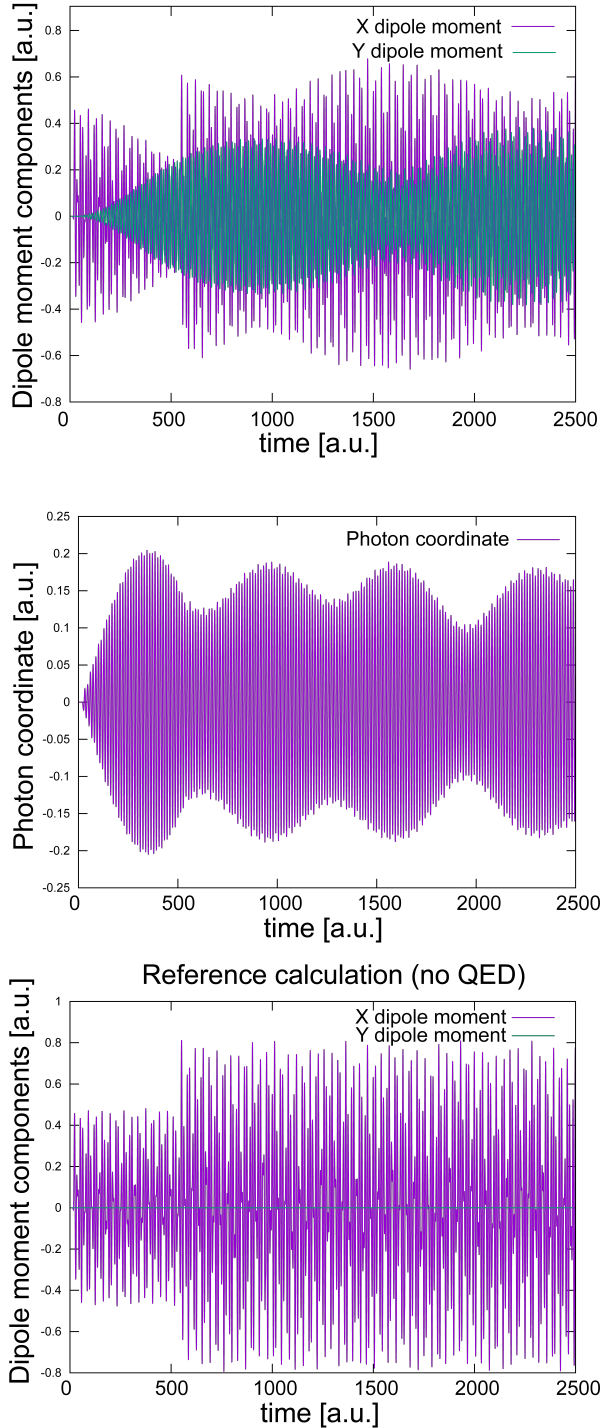


Figure 6: Dipole moment  $\mathbf{d}$  components (upper panel), photon coordinate  $\frac{\langle b^\dagger + b \rangle}{\sqrt{2\omega}}$  (middle panel), and reference dipole moment simulation (no QED, lower panel) for the dynamics of two perpendicular but identical  $\text{H}_2$  molecules at a distance of  $50 \text{ \AA}$ . The system is excited via two ultrashort pulses centered at  $t = 20 \text{ a.u.}$  and  $550 \text{ a.u.}$ , where the second pulse is switched on just before the maximal energy transfer between the two  $\text{H}_2$  molecules shown in Fig. 2.

simulation, the second pulse triggers a spontaneous emission as the system has lost energy after the interaction. Nevertheless, its effect is small enough that no sharp change in the dipole moment is shown in the last panel of Fig. 7.

Table 1: Energy of the  $(\text{H}_2)_2$  system before and after two ultrashort external electric pulses centered at  $t = 20 \text{ a.u.}$  and  $300 \text{ a.u.}$ . For the undressed electrons, the molecule oriented along  $y$  does not participate in the simulation, and the second pulse stimulates energy emission. In the QED simulation, after some energy has been transferred between the two  $\text{H}_2$  molecules, the second pulse (slightly) excites the molecule along  $x$  again.

Energy [a.u.]	Initial	Pulse 1	Pulse 2
RT-QED-CC	-2.32991	-2.31173	-2.31083
RT-CC	-2.32998	-2.31180	-2.31296

For the photon-dressed electrons, the molecules again gain energy from the pulse, as can be inferred from Tab. 1. In this case, the dipole moment along  $x$  still does not show a sudden envelope modification, but there is a sharp change in the envelope of the photon coordinate. As in Fig. 6, the amplitude of the photon coordinate oscillations does not reduce to zero, contrary to Fig. 2, which means that there is always a nonzero number of photons inside the cavity. However, the photon coordinate amplitude is larger than Fig. 6, and the second  $\text{H}_2$  molecule almost completely deexcites, contrary to the significant dipole moment along  $y$  shown in Fig. 6 after a complete oscillation. Therefore, these results show that multiple classical pulses can trigger nontrivial photon dynamics in a quantum optic device and alter the photon-mediated energy transfer between molecules in the strong coupling regime.

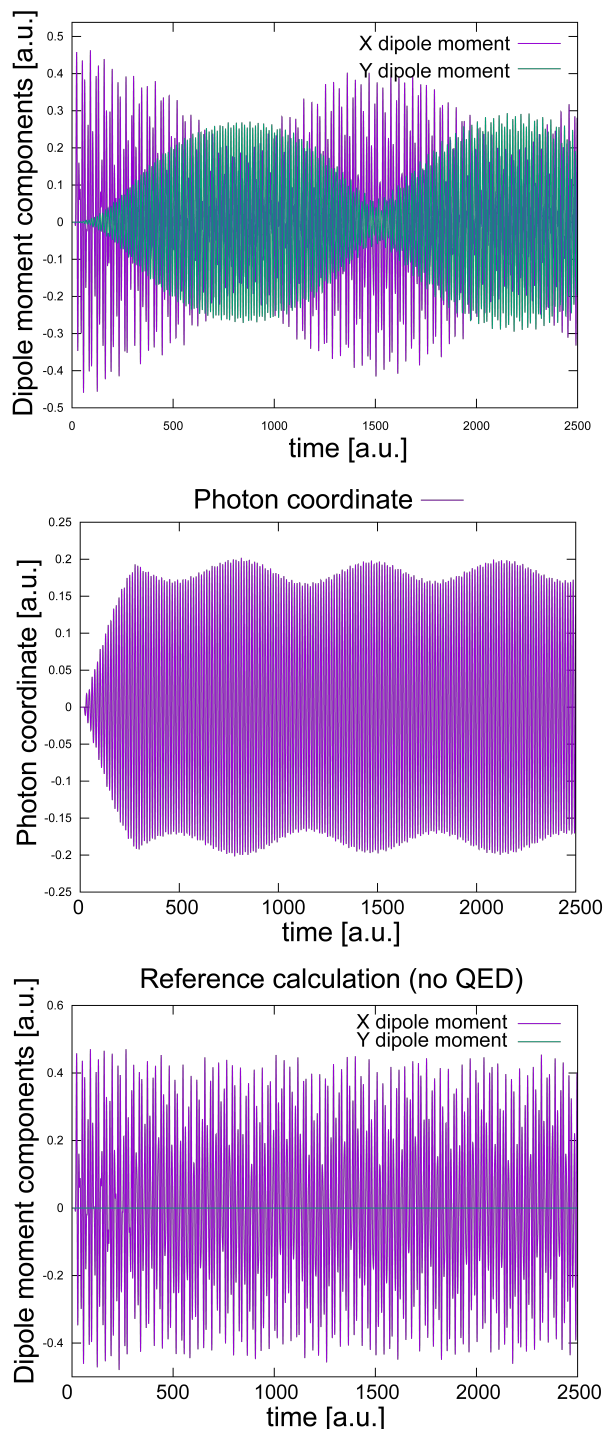


Figure 7: Dipole moment  $\mathbf{d}$  components (upper panel), photon coordinate  $\frac{\langle b^\dagger + b \rangle}{\sqrt{2\omega}}$  (middle panel), and reference dipole moment simulation (no QED, lower panel) for the dynamics of two perpendicular but identical  $\text{H}_2$  molecules at a distance of  $50 \text{ \AA}$ . The system is excited via two ultrashort pulses centered at  $t = 20 \text{ a.u.}$  and  $300 \text{ a.u.}$ , where the second pulse is switched on roughly at the maximum amplitude of the photon coordinate  $q$  shown in Fig. 2.

## Intramolecular electron-photon dynamics

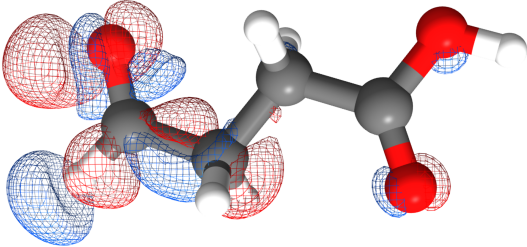
While we have focused so far on intermolecular energy transfer, the described effects apply equally to intramolecular processes. As a chemically interesting system, we focus on the succinic semialdehyde  $\text{C}_4\text{H}_6\text{O}_3$  illustrated in Fig. 8. In Fig. 8, we also report the transition density of three selected electronic excited states, whose excitation energy and dipole moments are reported in Tab. 2 (computational details and additional data can be found in the Supporting Information). The states I and III are

Table 2: Excitation energies and product of the CCSD left and right transition dipole moments along x, y, and z  $\langle L|d_p|CC \rangle \langle \Lambda|d_p|R \rangle$  for the excited states of the succinic semialdehyde  $\text{C}_4\text{H}_6\text{O}_3$  depicted in Fig. 8.

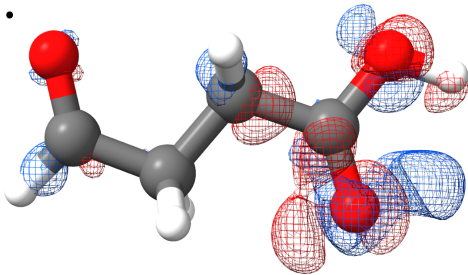
state	energy	x	y	z
I	7.144	0.0035	0.1041	0.0002
II	7.407	0.3813	0.0066	0.0000
III	7.802	0.1489	0.1681	0.0010

primarily associated with the aldehyde moiety, while the state II is an excitation of the acidic group. The molecule is then excited using a pulse centered at the energy of state II and polarized along x, thus coupling to the states II and III. For the QED simulation, the optical device is tuned to the undressed (out-of-cavity) excitation III reported in Tab. 2, with moderate coupling strength  $\lambda = 0.05 \text{ a.u.}$  and polarization along the xy-axis. The photon field is thus coupled to all 3 reported states, while the other excitations of the molecule are less relevant as they are highly detuned and carry lower transition dipoles. The inspection of the density displacement after the interaction with the pulse shows that both the aldehyde and the acid group are excited. The acidic moiety shows a more significant density displacement (and thus excitation), as expected since the pulse carrier frequency is tuned to state II and from its larger transition moment along x (see also the Supporting information). In the first panel of Fig. 9, we report the time evolution of the x and y components of the dipole

I.



II.



III.

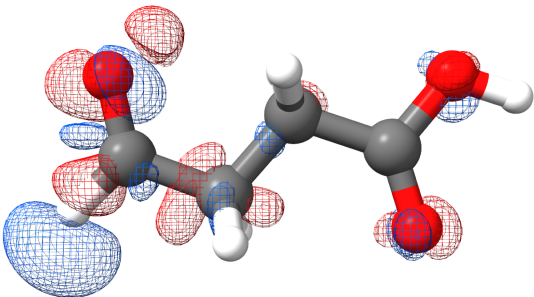


Figure 8: Ground to excited state transition densities for three selected excited states of the succinic semialdehyde  $C_4H_6O_3$ . The excitation energies and the transition moments are reported in Tab. 2. The states I and III are mainly associated with the aldehyde moiety, while the state II is an excitation of the acidic group.

moments inside (solid lines) and outside (reference, dotted lines) the cavity. The results clearly show larger fluctuations for the y dipole moment in the QED environment compared to the non-cavity case. The states I and III are thus more involved in the polaritonic system than in the purely electronic dynamics. In addition, the absorbed energies ( $5.554 \times 10^{-5}$  a.u. and  $4.640 \times 10^{-5}$  a.u. for the QED and reference electronic calculation, respectively) show a more favorable interaction of the external pulse with the polaritonic system. Therefore, the restructuring of the energy landscapes promoted by the light-matter strong coupling fundamentally changes the nature of the molecular excitation and can lead to more efficient interactions with external probes. In the second panel of Fig. 9, we report the photon coordinate computed for different quantum pictures: the QED-HF coherent state representation, the length gauge, and the velocity gauge. That is, the computed quantities are

$$\frac{\langle b^\dagger + b \rangle}{\sqrt{2\omega}}(t) \quad (26)$$

$$\frac{\langle b^\dagger + b - \sqrt{\frac{2}{\omega}} \boldsymbol{\lambda} \cdot \langle \mathbf{d} \rangle_{\text{QED-HF}} \rangle}{\sqrt{2\omega}}(t) \quad (27)$$

$$\frac{\langle b^\dagger + b + \sqrt{\frac{2}{\omega}} \boldsymbol{\lambda} \cdot (\mathbf{d} - \langle \mathbf{d} \rangle_{\text{QED-HF}}) \rangle}{\sqrt{2\omega}}(t). \quad (28)$$

While for the  $H_2$  system, the differences are less relevant, the permanent dipole moment of  $C_4H_6O_3$  effectively shifts the photon coordinate values. Fig. 9 thus shows that the picture changes have a fundamental effect in determining the values of photonic observables, and care must be taken when reporting theoretical simulations.<sup>39</sup> It is also interesting to notice that the fast oscillations of the photonic observables have an opposite sign of the oscillations in the y dipole moment, that is, they are dephased by  $\pi$ .

In addition, when the excited molecule transfers energy to the photon field, it can then be redistributed among all the states relevantly coupled to the optical device. The cavity field thus favors an energy redistribution from the acidic

moiety to the aldehyde group (long-range energy transfer) via the states I and III, and vice versa. Notice, however, that these transfers of

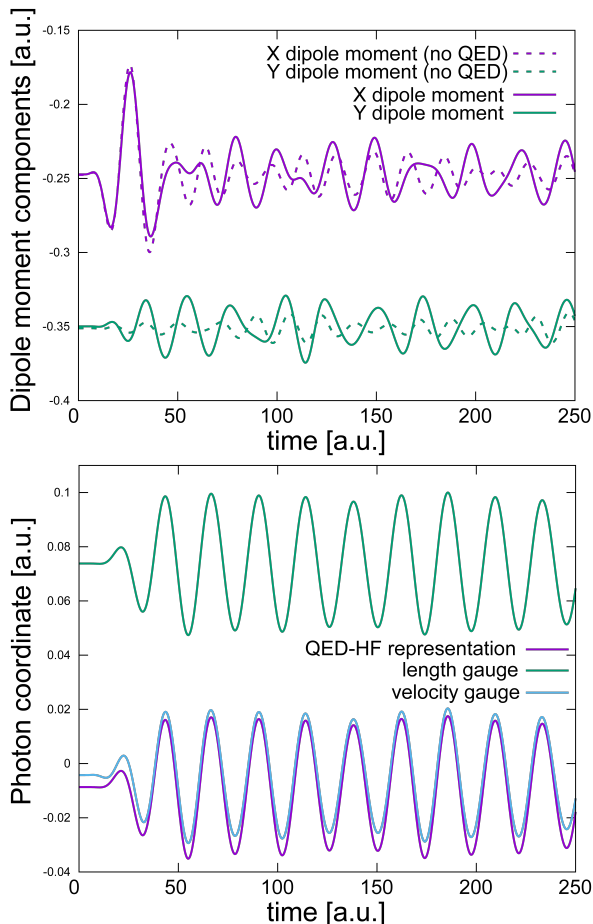


Figure 9: Time evolution of the x and y components of the dipole moment inside (solid lines) and outside (reference, dotted lines) the cavity for the succinic semialdehyde  $C_4H_6O_3$ . The cavity photon is resonant to the state II of Tab. 2, and its polarization is along the xy axis, and thus coupled to all 3 states. The enhanced fluctuations (compared to the reference calculation) along y prove a larger cavity-induced energy transfer from state II to states II and III.

excitations are not equally feasible: state II has a larger transition dipole moment than I, and thus its coupling to the photon field is favored. The cavity also promotes an excitation rearrangement of the aldehyde, transferring energy from state II to state I. The intramolecular energy transfer between distant moieties of a large molecule is a chemically relevant potential application of electronic strong coupling. We thus

speculate that electronic and vibrational strong coupling could affect charge migration and excitation transfer, which should be further investigated. In a sample with a large number of molecules, both inter- and intramolecular energy transfer would occur, and it might be challenging to separate the two effects. However, single-molecule (or few-molecules) light-matter strong coupling has been achieved in plasmonic cavities, and the developed ideas apply equally to such devices.

## Conclusions

In this paper, we have developed a real-time coupled cluster theory with quantized electromagnetic fields (RT-QED-CC). Our model can describe the real-time electron-photon dynamics of molecules coupled to optic devices such as microcavities or plasmonic structures, providing the time evolution of both matter and photon observables. Moreover, the CC parametrization includes both electron-photon and short-range electron-electron correlation. The method is thus also suited to study the interplay between the intermolecular forces and (collective) polaritonic environment, which is suggested to induce local chemical effects.<sup>53–55</sup> The *ab initio* description of light *and* matter can, in principle, be used to simulate the QED dynamics under both intense external fields (linear and nonlinear excitation regimes) and considerable light-matter coupling strengths (weak to ultrastrong coupling).

We use the developed method to investigate the electron-photon dynamics of polariton-mediated energy transfer processes, which can lead to advances in technologies such as solar cells. Our method allows for a microscopic description of the electron-photon dynamics, highlighting the light-matter interplay even on an attosecond scale. The QED-CC wave function gives us access to the dipole moments and the photon coordinate, which provide a clear quantitative description of the system’s evolution in the time domain. The spatial visualization of the transport process is also obtained from the charge density displacement.

Our results highlight different time scales in the matter and photon observables and furthermore prove the relevance of the dark states in such polaritonic processes. We discuss the requirements for photon-mediated energy transfer processes, which differ from the standard electronic Förster or Dexter mechanisms, and argue that such energy exchange processes can also be intramolecular, providing a channel alternative to molecular vibrations. We thus speculate that experimental investigations of intramolecular charge and energy migration under electronic and vibrational strong coupling could provide novel applications of polaritonic chemistry. Finally, we show that multiple classical pulses can alter the energy transfer dynamics and generate nontrivial dynamics of real photons inside the optical device. While our method is focused on electronic strong coupling (ESC), we believe the developed concepts are valid also for vibrational strong coupling (VSC).<sup>18,35–37</sup>

The developed method is well suited for supporting the study of experiments, including nonlinear optical processes,<sup>19–23</sup> quantum-light,<sup>26–32</sup> multi-photon, and transient absorption spectroscopies of molecules and molecular polaritons.<sup>10,11,33,34</sup> The study of nonlinear excitation regimes and pump-probe experiments in optical cavities will be investigated in future works, providing further insights into cavity-modified chemistry.

## Supporting Information

The Supporting Information includes the computational details of all the calculations, details on the RT-QED-CCSD-1 implementation in  $e^{\mathcal{T}}$ , and additional simulations of the systems under study.

## Data availability

Videos of the energy transfer dynamics and output files are available in the following repository DOI:10.5281/zenodo.10813660.

## Acknowledgements

M.C. acknowledges Andreas S. Skeidsvoll for insightful discussions. M.C. and H.K. acknowledge funding from the European Research Council (ERC) under the European Union’s Horizon 2020 Research and Innovation Programme (grant agreement No. 101020016). M. L. and H. K. acknowledge funding from the Department of Chemistry at the Norwegian University of Science and Technology (NTNU). E.R. acknowledges funding from the European Research Council (ERC) under the European Union’s Horizon Europe Research and Innovation Programme (Grant n. ERC-StG-2021-101040197 - QED-SPIN).

## References

- (1) Hutchison, J. A.; Schwartz, T.; Genet, C.; Devaux, E.; Ebbesen, T. W. Modifying chemical landscapes by coupling to vacuum fields. *Angewandte Chemie International Edition* **2012**, *51*, 1592–1596.
- (2) Munkhbat, B.; Wersäll, M.; Baranov, D. G.; Antosiewicz, T. J.; Shegai, T. Suppression of photo-oxidation of organic chromophores by strong coupling to plasmonic nanoantennas. *Science Advances* **2018**, *4*, eaas9552.
- (3) Thomas, A.; George, J.; Shalabney, A.; Dryzhakov, M.; Varma, S. J.; Moran, J.; Chervy, T.; Zhong, X.; Devaux, E.; Genet, C., et al. Ground-state chemical reactivity under vibrational coupling to the vacuum electromagnetic field. *Angewandte Chemie* **2016**, *128*, 11634–11638.
- (4) Lather, J.; Bhatt, P.; Thomas, A.; Ebbesen, T. W.; George, J. Cavity catalysis by cooperative vibrational strong coupling of reactant and solvent molecules. *Angewandte Chemie* **2019**, *131*, 10745–10748.
- (5) Thomas, A.; Lethuillier-Karl, L.; Nagarajan, K.; Vergauwe, R. M.; George, J.; Chervy, T.; Shalabney, A.; Devaux, E.; Genet, C.; Moran, J., et al. Tilting a

- ground-state reactivity landscape by vibrational strong coupling. *Science* **2019**, *363*, 615–619.
- (6) Canaguier-Durand, A.; Devaux, E.; George, J.; Pang, Y.; Hutchison, J. A.; Schwartz, T.; Genet, C.; Wilhelms, N.; Lehn, J.-M.; Ebbesen, T. W. Thermodynamics of molecules strongly coupled to the vacuum field. *Angewandte Chemie International Edition* **2013**, *52*, 10533–10536.
  - (7) Sau, A.; Nagarajan, K.; Patrahau, B.; Lethuillier-Karl, L.; Vergauwe, R. M.; Thomas, A.; Moran, J.; Genet, C.; Ebbesen, T. W. Modifying Woodward–Hoffmann stereoselectivity under vibrational strong coupling. *Angewandte Chemie International Edition* **2021**, *60*, 5712–5717.
  - (8) Hirai, K.; Takeda, R.; Hutchison, J. A.; Uji-i, H. Modulation of Prins cyclization by vibrational strong coupling. *Angewandte Chemie* **2020**, *132*, 5370–5373.
  - (9) Ahn, W.; Triana, J. F.; Recabal, F.; Herrera, F.; Simpkins, B. S. Modification of ground-state chemical reactivity via light–matter coherence in infrared cavities. *Science* **2023**, *380*, 1165–1168.
  - (10) Wang, H.; Wang, H.-Y.; Sun, H.-B.; Cerea, A.; Toma, A.; De Angelis, F.; Jin, X.; Razzari, L.; Cojoc, D.; Catone, D., et al. Dynamics of strongly coupled hybrid states by transient absorption spectroscopy. *Advanced Functional Materials* **2018**, *28*, 1801761.
  - (11) Wang, K.; Nagarajan, K.; Kushida, S.; Kulangara, S.; Genet, C.; Ebbesen, T. Study of the selection rules of molecular polaritonic transitions by two-photon absorption spectroscopy. **2023**,
  - (12) Georgiou, K.; Jayaprakash, R.; Othonos, A.; Lidzey, D. G. Ultralong-Range Polariton-Assisted Energy Transfer in Organic Microcavities. *Angewandte Chemie* **2021**, *133*, 16797–16803.
  - (13) Zhong, X.; Chervy, T.; Zhang, L.; Thomas, A.; George, J.; Genet, C.; Hutchison, J. A.; Ebbesen, T. W. Energy transfer between spatially separated entangled molecules. *Angewandte Chemie* **2017**, *129*, 9162–9166.
  - (14) Zhong, X.; Chervy, T.; Wang, S.; George, J.; Thomas, A.; Hutchison, J. A.; Devaux, E.; Genet, C.; Ebbesen, T. W. Non-Radiative Energy Transfer Mediated by Hybrid Light-Matter States. *Angewandte Chemie* **2016**, *128*, 6310–6314.
  - (15) Cargioli, A.; Lednev, M.; Lavista, L.; Camposeo, A.; Sassella, A.; Pisignano, D.; Tredicucci, A.; Garcia-Vidal, F. J.; Feist, J.; Persano, L. Active control of polariton-enabled long-range energy transfer. *Nanophotonics* **2024**,
  - (16) Coles, D. M.; Somaschi, N.; Michetti, P.; Clark, C.; Lagoudakis, P. G.; Savvidis, P. G.; Lidzey, D. G. Polariton-mediated energy transfer between organic dyes in a strongly coupled optical microcavity. *Nature materials* **2014**, *13*, 712–719.
  - (17) Schäfer, C.; Ruggenthaler, M.; Appel, H.; Rubio, A. Modification of excitation and charge transfer in cavity quantum-electrodynamical chemistry. *Proceedings of the National Academy of Sciences* **2019**, *116*, 4883–4892.
  - (18) Xiang, B.; Ribeiro, R. F.; Du, M.; Chen, L.; Yang, Z.; Wang, J.; Yuen-Zhou, J.; Xiong, W. Intermolecular vibrational energy transfer enabled by microcavity strong light–matter coupling. *Science* **2020**, *368*, 665–667.
  - (19) Wang, K.; Seidel, M.; Nagarajan, K.; Chervy, T.; Genet, C.; Ebbesen, T. Large optical nonlinearity enhancement under electronic strong coupling. *Nature Communications* **2021**, *12*, 1486.
  - (20) Ge, F.; Han, X.; Xu, J. Strongly coupled systems for nonlinear optics. *Laser & Photonics Reviews* **2021**, *15*, 2000514.



- (21) Chervy, T.; Xu, J.; Duan, Y.; Wang, C.; Mager, L.; Frerejean, M.; Munninghoff, J. A.; Tinnemans, P.; Hutchison, J. A.; Genet, C., et al. High-efficiency second-harmonic generation from hybrid light-matter states. *Nano letters* **2016**, *16*, 7352–7356.
- (22) Malave, J.; Ahrens, A.; Pitagora, D.; Covington, C.; Varga, K. Real-space, real-time approach to quantum-electrodynamical time-dependent density functional theory. *The Journal of chemical physics* **2022**, *157*.
- (23) Xiang, B.; Ribeiro, R. F.; Li, Y.; Dunkelberger, A. D.; Simpkins, B. B.; Yuen-Zhou, J.; Xiong, W. Manipulating optical nonlinearities of molecular polaritons by delocalization. *Science advances* **2019**, *5*, eaax5196.
- (24) Haugland, T. S.; Ronca, E.; Kjønstad, E. F.; Rubio, A.; Koch, H. Coupled cluster theory for molecular polaritons: Changing ground and excited states. *Physical Review X* **2020**, *10*, 041043.
- (25) Helgaker, T.; Jørgensen, P.; Olsen, J. *Molecular electronic-structure theory*; John Wiley & Sons, 2013.
- (26) Dorfman, K. E.; Schlawin, F.; Mukamel, S. Nonlinear optical signals and spectroscopy with quantum light. *Reviews of Modern Physics* **2016**, *88*, 045008.
- (27) Schlawin, F.; Mukamel, S. Two-photon spectroscopy of excitons with entangled photons. *The Journal of chemical physics* **2013**, *139*.
- (28) Ruggenthaler, M.; Tancogne-Dejean, N.; Flick, J.; Appel, H.; Rubio, A. From a quantum-electrodynamical light-matter description to novel spectroscopies. *Nature Reviews Chemistry* **2018**, *2*, 1–16.
- (29) Raymer, M. G.; Landes, T.; Marcus, A. H. Entangled two-photon absorption by atoms and molecules: A quantum optics tutorial. *The Journal of Chemical Physics* **2021**, *155*.
- (30) Schlawin, F.; Dorfman, K. E.; Mukamel, S. Entangled two-photon absorption spectroscopy. *Accounts of chemical research* **2018**, *51*, 2207–2214.
- (31) Rezus, Y.; Walt, S.; Lettow, R.; Renn, A.; Zumofen, G.; Götzinger, S.; Sandoghdar, V. Single-photon spectroscopy of a single molecule. *Physical review letters* **2012**, *108*, 093601.
- (32) Raimond, J.-M.; Brune, M.; Haroche, S. Manipulating quantum entanglement with atoms and photons in a cavity. *Reviews of Modern Physics* **2001**, *73*, 565.
- (33) Gu, B.; Gu, Y.; Chernyak, V. Y.; Mukamel, S. Cavity Control of Molecular Spectroscopy and Photophysics. *Accounts of Chemical Research* **2023**, *56*, 2753–2762.
- (34) DelPo, C. A.; Kudisch, B.; Park, K. H.; Khan, S.-U.-Z.; Fassioli, F.; Fausti, D.; Rand, B. P.; Scholes, G. D. Polariton transitions in femtosecond transient absorption studies of ultrastrong light-molecule coupling. *The journal of physical chemistry letters* **2020**, *11*, 2667–2674.
- (35) Cao, J. Generalized resonance energy transfer theory: Applications to vibrational energy flow in optical cavities. *The Journal of Physical Chemistry Letters* **2022**, *13*, 10943–10951.
- (36) Tibben, D. J.; Bonin, G. O.; Cho, I.; Lakhwani, G.; Hutchison, J.; Gómez, D. E. Molecular energy transfer under the strong light-matter interaction regime. *Chemical Reviews* **2023**, *123*, 8044–8068.
- (37) Li, T. E.; Nitzan, A.; Subotnik, J. E. Collective vibrational strong coupling effects on molecular vibrational relaxation and

- energy transfer: Numerical insights via cavity molecular dynamics simulations. *Angewandte Chemie* **2021**, *133*, 15661–15668.
- (38) Ruggenthaler, M.; Sidler, D.; Rubio, A. Understanding polaritonic chemistry from ab initio quantum electrodynamics. *Chemical Reviews* **2023**, *123*, 11191–11229.
- (39) Castagnola, M.; Riso, R. R.; Barlini, A.; Ronca, E.; Koch, H. Polaritonic response theory for exact and approximate wave functions. *Wiley Interdisciplinary Reviews: Computational Molecular Science* **2024**, *14*, e1684.
- (40) Pedersen, T. B.; Koch, H. Coupled cluster response functions revisited. *The Journal of chemical physics* **1997**, *106*, 8059–8072.
- (41) Koch, H.; Jorgensen, P. Coupled cluster response functions. *The Journal of chemical physics* **1990**, *93*, 3333–3344.
- (42) Sverdrup Ofstad, B.; Aurbakken, E.; Sigmundson Schøyen, Ø.; Kristiansen, H. E.; Kvaal, S.; Pedersen, T. B. Time-dependent coupled-cluster theory. *Wiley Interdisciplinary Reviews: Computational Molecular Science* **2023**, *13*, e1666.
- (43) Skeidsvoll, A. S.; Balbi, A.; Koch, H. Time-dependent coupled-cluster theory for ultrafast transient-absorption spectroscopy. *Physical Review A* **2020**, *102*, 023115.
- (44) Skeidsvoll, A. S.; Moitra, T.; Balbi, A.; Paul, A. C.; Coriani, S.; Koch, H. Simulating weak-field attosecond processes with a Lanczos reduced basis approach to time-dependent equation-of-motion coupled-cluster theory. *Physical Review A* **2022**, *105*, 023103.
- (45) Nascimento, D. R.; DePrince, A. E. A general time-domain formulation of equation-of-motion coupled-cluster theory for linear spectroscopy. *The Journal of Chemical Physics* **2019**, *151*.
- (46) Pedersen, T. B.; Kvaal, S. Symplectic integration and physical interpretation of time-dependent coupled-cluster theory. *The Journal of chemical physics* **2019**, *150*.
- (47) Huber, C.; Klamroth, T. Explicitly time-dependent coupled cluster singles doubles calculations of laser-driven many-electron dynamics. *The Journal of chemical physics* **2011**, *134*.
- (48) Aurbakken, E.; Kristiansen, H.; Kvaal, S.; Pedersen, T., et al. Time-dependent coupled-cluster theory. *Wiley Interdiscip. Rev.: Comput. Mol. Sci.* **2023**, *13*, e1666.
- (49) Schlawin, F. Entangled photon spectroscopy. *Journal of Physics B: Atomic, Molecular and Optical Physics* **2017**, *50*, 203001.
- (50) Folkestad, S. D.; Kjønstad, E. F.; Myhre, R. H.; Andersen, J. H.; Balbi, A.; Coriani, S.; Giovannini, T.; Goletto, L.; Haugland, T. S.; Hutcheson, A., et al. e T 1.0: An open source electronic structure program with emphasis on coupled cluster and multilevel methods. *The Journal of Chemical Physics* **2020**, *152*, 184103.
- (51) Scholes, G. D. Long-range resonance energy transfer in molecular systems. *Annual review of physical chemistry* **2003**, *54*, 57–87.
- (52) Skeidsvoll, A. S.; Koch, H. Comparing real-time coupled-cluster methods through simulation of collective Rabi oscillations. *Physical Review A* **2023**, *108*, 033116.
- (53) Castagnola, M.; Haugland, T. S.; Ronca, E.; Koch, H.; Schäfer, C. Collective strong coupling modifies aggregation and solvation. *The Journal of Physical Chemistry Letters* **2024**, *15*, 1428–1434.
- (54) Biswas, S.; Mondal, M.; Chandrasekharan, G.; Singh, A.; Thomas, A. Electronic

Strong Coupling Modifies the Ground-state Intermolecular Interactions in Chlorin Thin Films. **2024**,

- (55) Haugland, T. S.; Schäfer, C.; Ronca, E.; Rubio, A.; Koch, H. Intermolecular interactions in optical cavities: An ab initio QED study. *The Journal of Chemical Physics* **2021**, *154*, 094113.

# **Supplemental Information: Strong coupling electron-photon dynamics: a real-time investigation of energy redistribution in molecular polaritons**

Matteo Castagnola,<sup>†</sup> Marcus T. Lexander,<sup>†</sup> Enrico Ronca,<sup>\*,‡</sup> and Henrik Koch<sup>\*,†</sup>

*<sup>†</sup>Department of Chemistry, Norwegian University of Science and Technology, 7491*

*Trondheim, Norway*

*<sup>‡</sup>Dipartimento di Chimica, Biologia e Biotechnologie, Università degli Studi di Perugia, Via*

*Elce di Sotto, 8,06123, Perugia, Italy*

E-mail: enrico.ronca@unipg.it; henrik.koch@ntnu.no

# Contents

<b>S1 Computational details</b>	<b>S2</b>
<b>S2 Implementation of the RT-QED-CC equations</b>	<b>S3</b>
<b>S3 Additional results</b>	<b>S5</b>
S3.1 Additional (H <sub>2</sub> ) <sub>2</sub> data . . . . .	S5
S3.2 Additional succinic semialdehyde C <sub>4</sub> H <sub>6</sub> O <sub>3</sub> data . . . . .	S10
<b>S4 Real-time QED-CC equations</b>	<b>S12</b>
<b>S5 Molecular geometries</b>	<b>S14</b>
<b>References</b>	<b>S17</b>

## S1 Computational details

All the calculations have been performed with a private branch of the  $e^{\mathcal{T}}$  program.<sup>1</sup> Videos of the energy transfer dynamics and output files are available in a Zenodo repository DOI: [10.5281/zenodo.10813660](https://doi.org/10.5281/zenodo.10813660)

The (H<sub>2</sub>)<sub>2</sub> system is described in the 6-31++g\*\* basis set, with one H<sub>2</sub> oriented along the x axis and the other on the y axis. The molecular geometries are reported in section S5. The system is excited with an external pulse

$$\mathbf{E}(t) = \mathcal{E}(t) \cos(\omega_e t + \phi) \quad (1)$$

with carrier frequency  $\omega_e = 0.464\,408\,577$  a.u. (resonant to the first bright excitation of one H<sub>2</sub>) and phase shift  $\phi = 0$ . The envelope function  $\mathcal{E}(t)$  is a gaussian with maximum intensity  $\mathcal{E}_0 = 0.05$  a.u. and width 2.0 a.u., polarized along x. The equations are propagated for at least 2000 a.u. of time using a Runge-Kutta integrator with a time step of 0.005 a.u., and

the energies, the dipole moments, photon coordinate, amplitudes, multipliers, electric field, and density matrices are recorded every 0.25 a.u.. The densities are visualized on the xy plane by using the density matrices to construct a cube file on a grid of 0.1 Å spacing, and the ground state density was subtracted to the density of each snapshot to obtain the density displacement. The QED photon field is tuned to the H<sub>2</sub> excitation energy ( $\omega = 0.464\,408\,577$  a.u.) and polarization along the xy bisector line  $\epsilon = (\frac{1}{\sqrt{2}}, \frac{1}{\sqrt{2}}, 0)$ . The light-matter coupling strength is  $\lambda = 0.01$  a.u. unless stated otherwise, and we consider a single photon mode. In this way, the photon field is coupled to both hydrogens, but the external pulse only excites one of them.

The succinic semialdehyde C<sub>4</sub>H<sub>6</sub>O<sub>3</sub> is studied in the 6-31g\* basis set and oriented such that the carbon and oxygens of the acidic group lie in the xy plane (the aldehydic group is also *almost* lying in the same plane). The molecular geometry is reported in section S5 in Table S11. The system is excited with an external pulse as in Equation 1, but we used a sine-squared envelope function. The carrier angular frequency now is  $\omega_e = 0.272\,216\,406\,0$  a.u. (resonant to the excitation II reported in the main text, mainly localized on the acid group) and phase shift  $\phi = 0$ , with a peak strength of  $\mathcal{E}_0 = 0.001$  a.u., width 45.0 a.u., and polarized along x. The equations are propagated for at least 250 a.u. of time using a Runge-Kutta integrator with a time step of 0.005 a.u., and the energies, the dipole moments, photon coordinate, amplitudes, multipliers, electric field, and density matrices are recorded every 0.25 a.u.. The QED photon field is tuned to the excitation III reported in the main text (mainly localized on the aldehyde)  $\omega = 0.286\,743\,5$  a.u. with light-matter coupling strength  $\lambda = 0.05$  a.u. and polarized along  $\epsilon = (\frac{1}{\sqrt{2}}, \frac{1}{\sqrt{2}}, 0)$ .

## S2 Implementation of the RT-QED-CC equations

The RT-QED-CCSD-1 equations have been implemented in a development version of the  $e^{\mathcal{T}}$  program.<sup>1</sup> For debugging purposes, we cannot resort to a real-time QED-FCI implementation

since, even for two-electron systems like  $\text{H}_2$ ,  $\text{HHe}^+$ , and  $\text{He}$ , the photon degrees of freedom are modeled differently. QED-FCI relies on a CI truncation of the photon Fock space, while the exponential of the photon excitation in QED-CC  $e^{\gamma b^\dagger}$  is similar to a photon coherent state, having components in the whole photon Fock space. The QED-FCI and QED-CC results are thus different also for two-electron systems. We must then find a different path to prove the correctness of our implementation.

First, our implementation for quenched light-matter coupling strength  $\lambda = 0$  recovers the RT-CCSD dynamics. Although necessary, this is clearly not enough. Therefore, we follow the ideas presented in Ref.<sup>2</sup> and implement a propagation of the RT-QED-CCSD-1 equations in imaginary time, that is, with the substitution  $t \rightarrow -it$ . An eigenstate of energy  $E'$  of the Hamiltonian evolves in time, only changing its global phase  $e^{-iE't} \rightarrow e^{-E't}$ , and therefore, the excited states will show a faster exponential decay than the ground state.<sup>3</sup> Moreover, the CC parametrization always ensures an intermediate normalization

$$\langle HF|e^T|HF\rangle = 1, \tag{2}$$

and thus, no renormalization is necessary. Therefore, regardless of the initial amplitudes, after enough time has passed on the imaginary time propagation simulation, the state will decay onto the QED-CC ground state. This is readily verified with our implementation of the RT-QED-CCSD-1, and in Figure S1 we report the energy of the imaginary time propagation for an  $\text{H}_2\text{O}$  molecule in an optical cavity of frequency  $\omega = 0.371\,048$  a.u. with light-matter coupling strength  $\lambda = 0.1$  a.u. and polarization along the  $C_2$  axis of the molecule, using the 6-31g\* basis set. The initial state of the simulation is the QED-HF state, corresponding to the cluster operator  $T = 0$  and Lagrange multipliers  $\bar{t}_{\mu n} = 0$ , which is then propagated for 30 a.u. of time with a time step of 0.01 a.u. using a Runge-Kutta integrator. The energy of the system (panel B in Figure S1) quickly converges to the QED-CCSD ground state energy, and so do the amplitudes, the Lagrange multipliers, and molecular properties such as the permanent

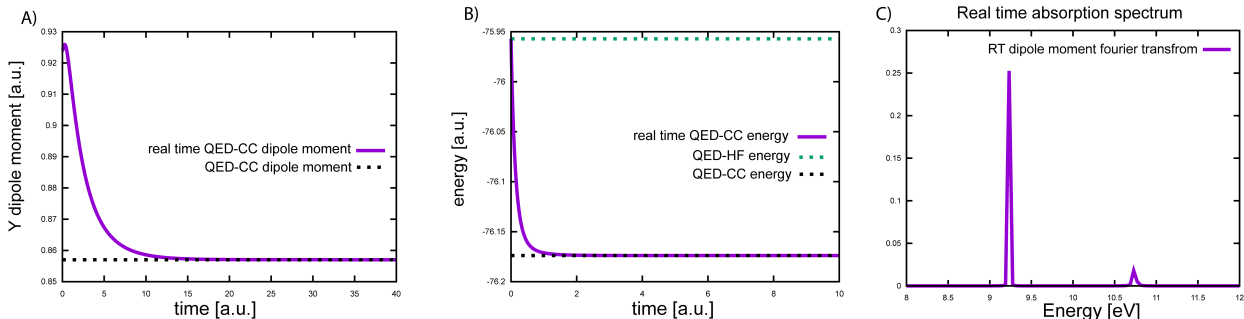


Figure S1: A)  $y$  component of the dipole moment of a 6-31g\* water molecule starting from the QED-HF state and propagating over imaginary time  $t \rightarrow it$ . The dipole moment quickly converges to the ground state QED-CCSD expectation value. B) Energy of a 6-31g\* water molecule starting from the QED-HF state and propagating over imaginary time  $t \rightarrow it$ . The energy quickly converges to the QED-CCSD ground state energy. C) Absorption spectrum of a 6-31g\* water molecule after excitation with a short electric pulse computed via fast Fourier transform of the propagation of the  $y$  component of the dipole moment. The excitation energies and the intensities are consistent with the EOM-QED-CCSD-1 calculations.

dipole moment (panel A in Figure S1) and the photon coordinate. Finally, performing a simulation in real-time (no imaginary time propagation) following the excitation of the system with an electric pulse (central time 1.0 a.u., carrier angular frequency 0.371 048 a.u., peak intensity 0.05 a.u., width 0.2 a.u., polarized along the  $C_2$  axis of water), we can compute the absorption spectrum by a fast Fourier transform of the dipole moment. The spectrum is reported in panel C of Figure S1 after propagating the system for 4000.0 a.u., and the computed peaks and intensities agree with the EOM-QED-CCSD-1 simulation.

## S3 Additional results

In this section, we include additional results for the systems discussed in the main text.

### S3.1 Additional $(\text{H}_2)_2$ data

In Figure S2, we report the dipole moments after exciting the  $(\text{H}_2)_2$  system with an external pulse. The left panels refer to the geometry in Table S9 while the right panels refer to the geometry in Table S10, with light-matter coupling strengths  $\lambda = 0.01$  a.u. and 0.005 a.u. (top



to bottom respectively). The time scale of the photon-mediated energy transfer is reduced by a factor of 2 in the simulations with  $\lambda = 0.005$  a.u. compared to  $\lambda = 0.01$  a.u.. This result is reasonable as the photon-mediated time scales are determined by the Rabi splittings, which are almost linear in  $\lambda$ . Notice, however, that the introduction of intermolecular interactions effectively detunes the cavity from the molecular excitations, so the behavior is not expected to be perfectly linear. The dipole self-energy, although small, generates a similar detuning effect. Nevertheless, in about twice the time compared to  $\lambda = 0.01$  a.u., the same amount of

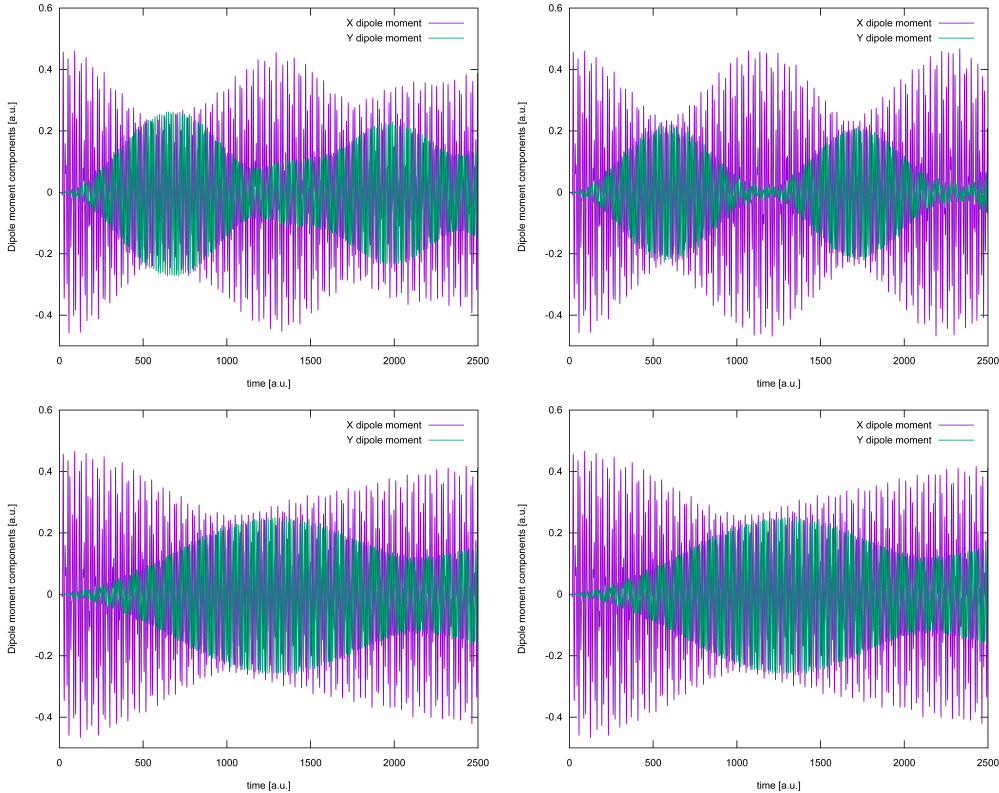


Figure S2: Dipole moments after exciting the  $(\text{H}_2)_2$  system with an external pulse. The left panels refer to the geometry in Table S9 while the right panels refer to the geometry in Table S10. In the upper panels, the light-matter coupling strength is set to 0.01 a.u. as in the figures in the main text, while the lower panels are computed using  $\lambda = 0.005$  a.u. and therefore have different time scales.

energy transfer can be achieved (if decoherence processes are suppressed). On the other hand, the electronic energy transfer (Förster and Dexter) is almost unaffected by any modification of the properties of the optic device (the dipole self-energy here only introduces a tiny shift

of the molecular energies). The same conclusions can be drawn from the photon coordinate, plotted in Figure S3 for the  $(\text{H}_2)_2$  system of Table S9. Notice that no energy transfer occurs

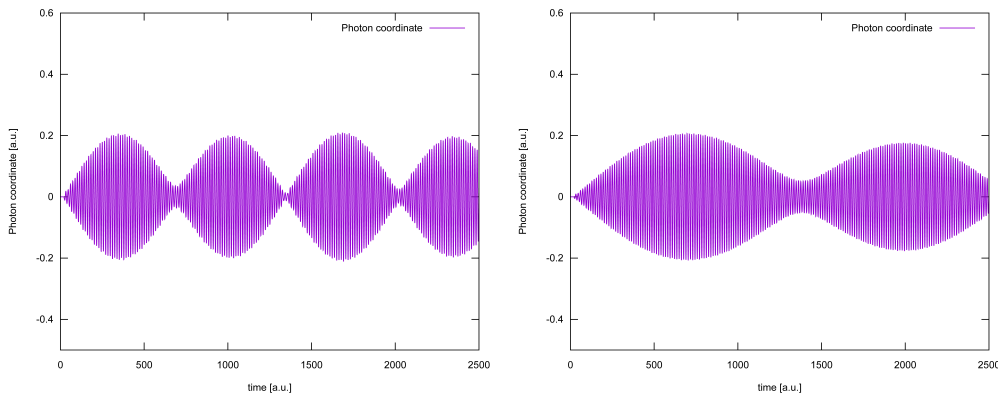


Figure S3: Photon coordinate after exciting the  $(\text{H}_2)_2$  system with geometry in Table S9. The left panel and right panels are computed using  $\lambda = 0.01$  a.u. and  $0.005$  a.u. respectively, and therefore have different time scales.

without the mediation of the cavity photon, as seen from the out-of-cavity simulation in

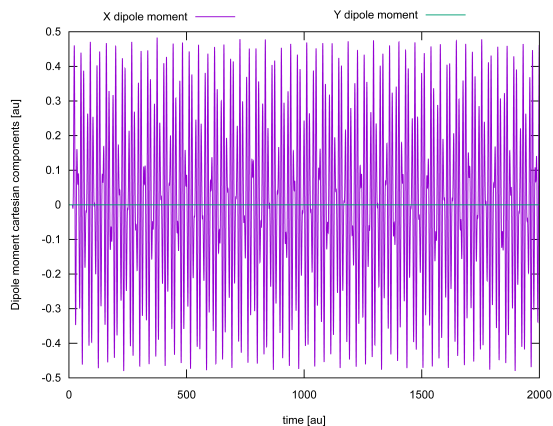


Figure S4: Dipole moment after exciting the  $(\text{H}_2)_2$  system with geometry in Table S9 outside the cavity (no QED).

It is also interesting to investigate how these quantities would change by increasing the number of replicas in the simulation  $((\text{H}_2)_2)_N$  while rescaling the coupling strength by  $1/\sqrt{N}$ , thus keeping the Rabi splitting constant. In Figure S5, we report the computed dipole moments and photon coordinates, and in Table S5 we report the energies of the system before and after the interaction with the pulse for  $N = 2$  and  $3$ . All the systems are subject

to the same electric pulse described in section S1. The energy gained from the interaction

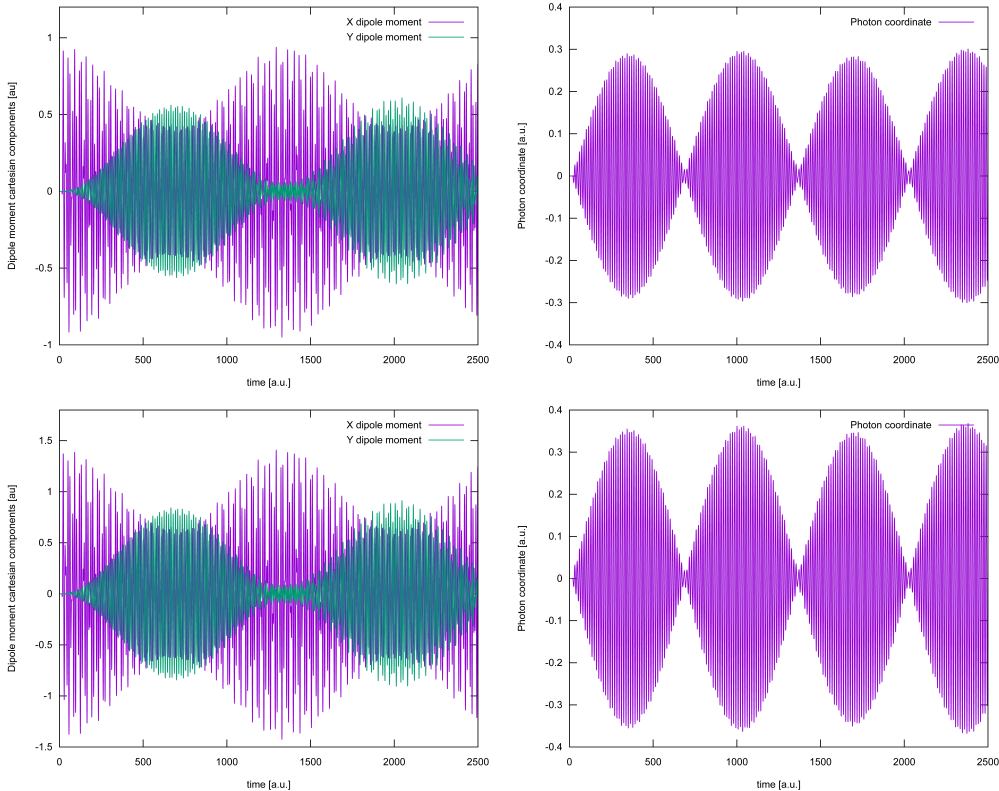


Figure S5: Dipole moment and photon coordinate for two (upper panels) and three (lower panels) identical  $(\text{H}_2)_2$  systems (placed at  $300 \text{ \AA}$  distance and with geometry in Table S7) after excitation with the same pulse as Figure S2. The coupling strength has been rescaled by a factor of  $1/\sqrt{2}$  and  $1/\sqrt{3}$  to  $\lambda = 0.007\,071\,067\,8 \text{ a.u.}$  and  $0.005\,773\,502\,6 \text{ a.u.}$  to keep the Rabi splitting constant.

with the external pulse increases linearly with the number of replicas  $N$ , as expected since the energy absorption depends on the number of interacting molecules (the size-intensivity and extensivity of the CC parametrization are a fundamental aspect of the theory). This is also reflected in the linear  $N$  scaling of the oscillation amplitude of the dipole moment in Figure S5 (see the main text for the results of a single  $(\text{H}_2)_2$ ). In addition, the time scales are the same in these simulations, as expected, since they show the same Rabi splitting. The time scales, therefore, are only determined by the *collective* coupling strength  $\lambda\sqrt{N}$ . On the other hand, the amplitudes of the photonic properties scale as the square root  $\sqrt{N}$  of the number of replicas, which suggests that a relevant amount of energy is stored in the dark

states. Therefore, photon and matter quantities have a different scaling with the number of replicas, when all the systems are subject to the same external pulse. The same conclusions are drawn for the  $(\text{H}_2)_2$  system with slightly different bond length (geometry in Table S8), as reported in Figure S6

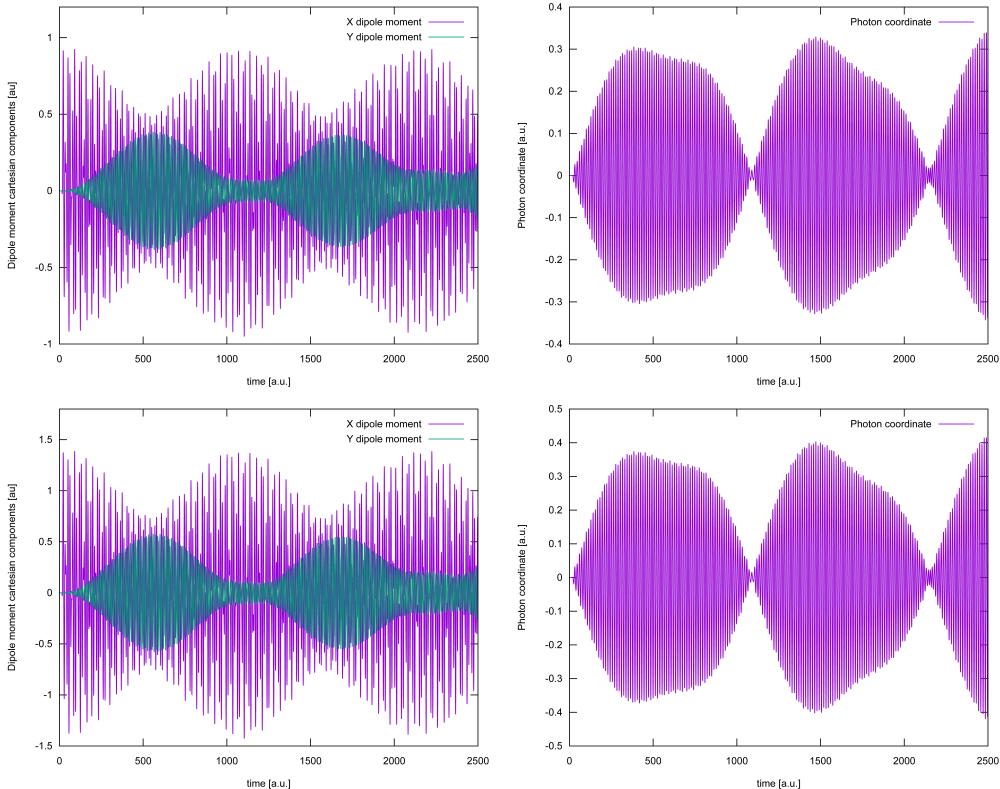


Figure S6: Dipole moment and photon coordinate for two (upper panels) and three (lower panels) identical  $(\text{H}_2)_2$  systems (placed at  $300 \text{ \AA}$  distance and with geometry in Table S8) after excitation with the same pulse as Figure S2. The coupling strength has been rescaled by a factor of  $1/\sqrt{2}$  and  $1/\sqrt{3}$  to  $\lambda = 0.0070710678 \text{ a.u.}$  and  $0.0057735026 \text{ a.u.}$  to keep the Rabi splitting constant.

In Table S1, we report the energy of the  $(\text{H}_2)_2$  system of Table S7 (identical perpendicular hydrogens,  $D = 50 \text{ \AA}$ ) before and after the interaction with the external pulse.

**Table S1: Energy of the  $(\text{H}_2)_2$  system of Table S7 before and after before and after the interaction with the external pulse. Computational details are reported in section S1**

Energy [a.u.]	Initial	Pulse 1
QED simulation	-2.32991	-2.31173

In Table S2, we report the energy of the  $(\text{H}_2)_2$  system of Table S8 (perpendicular hydrogens of bond lengths 0.76 Å and 0.78 Å,  $D = 50$  Å) before and after the interaction with the external pulse.

**Table S2: Energy of the  $(\text{H}_2)_2$  system of Table S8 before and after before and after the interaction with the external pulse. Computational details are reported in section S1**

Energy [a.u.]	Initial	Pulse 1
QED simulation	-2.32914	-2.31096

In Table S3, we report the energy of the  $(\text{H}_2)_2$  system of Table S9 (identical perpendicular hydrogens,  $D = 5$  Å) before and after the interaction with the external pulse.

**Table S3: Energy of the  $(\text{H}_2)_2$  system of Table S9 before and after before and after the interaction with the external pulse. Computational details are reported in section S1**

Energy [a.u.]	Initial	Pulse 1
QED simulation	-2.32993	-2.31176

In Table S4, we report the energy of the  $(\text{H}_2)_2$  system of Table S10 (perpendicular hydrogens of bond lengths 0.76 Å and 0.78 Å,  $D = 5$  Å) before and after the interaction with the external pulse.

**Table S4: Energy of the  $(\text{H}_2)_2$  system of Table S10 before and after before and after the interaction with the external pulse. Computational details are reported in section S1**

Energy [a.u.]	Initial	Pulse 1
QED simulation	-2.32916	-2.31099

In Table S5, we report the energy of the  $(\text{H}_2)_2$  system of Figure S5 before and after the interaction with the external pulse.

### S3.2 Additional succinic semialdehyde $\text{C}_4\text{H}_6\text{O}_3$ data

In Figure S7, we report selected snapshots of the density displacement (compared to the ground state) in the xy plane following the interaction with the external pulse described in

**Table S5: Energy of the  $(\text{H}_2)_2$  system of Figure S5 before and after before and after the interaction with the external pulse. Computational details are reported in section S1**

Energy [a.u.]	Initial	Pulse 1	Difference [a.u.]
QED simulation: 2 replicas	-4.65989	-4.62354	0.03635
QED simulation: 3 replicas	-6.98988	-6.93535	0.05453

section S1 for the succinic semialdehyde  $\text{C}_4\text{H}_6\text{O}_3$  in an optical cavity.<sup>1</sup> The figure also shows

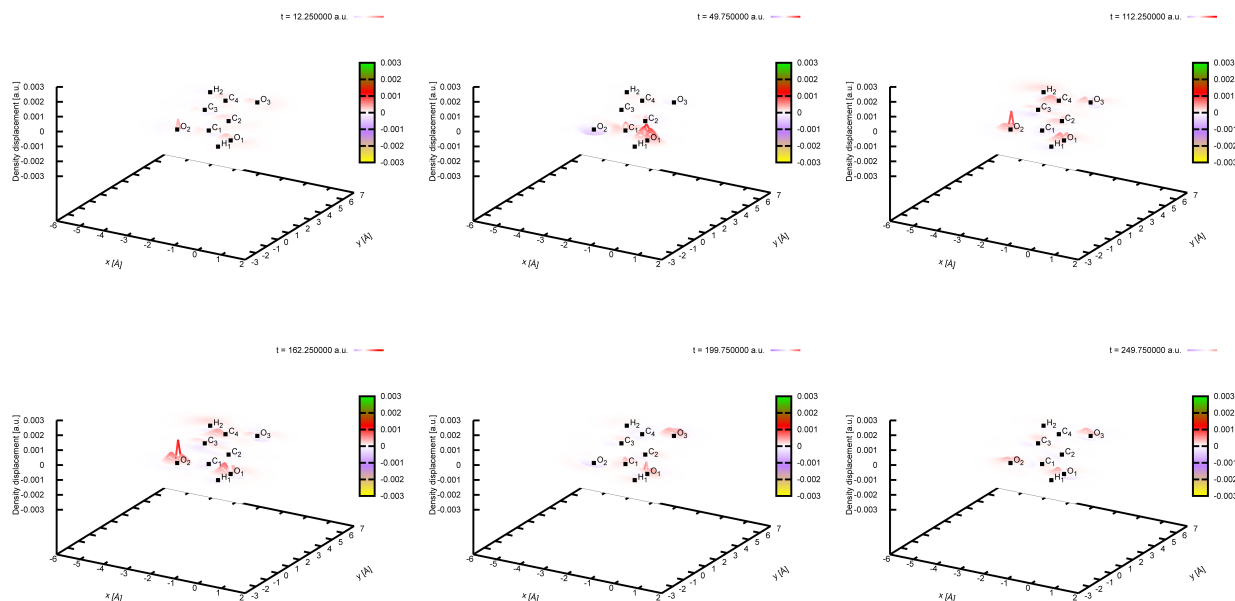


**Figure S7: Electronic displacement for the succinic semialdehyde  $\text{C}_4\text{H}_6\text{O}_3$  in an optical cavity following the excitation with an external pulse.**

the projection of the aldehyde group and the carbon chain on the xy plane (the COO atoms of the acid group lie in the plane while the aldehyde group has small components on z as well, see Table S11). After the pulse has passed, the excitation is mainly localized on the acid group. Compared to the standard (no QED) electronic dynamics, the cavity favors the interaction with the external pulse as more energy is absorbed (see Table S6). As shown in the main text, the electron dynamics is thus fundamentally modified with similar dipole oscillations on x and more intense oscillations on y. The cavity favors a mixing of the states

<sup>1</sup>Videos of the energy-transfer dynamics are available in the following repository: DOI:10.5281/zenodo.10813660.

II and III (and partially I), and the two arising middle polaritons have an energy that is closer to the pulse carrier, which favors the interaction with the external pulse.

In Table S6, we report the energy of the succinic semialdehyde  $C_4H_6O_3$  of Table S11 before and after the interaction with the external pulse.

**Table S6: Energy of the succinic semialdehyde  $C_4H_6O_3$  of Table S11 before and after before and after the interaction with the external pulse. Computational details are reported in section S1**

Energy [a.u.]	Initial	Pulse 1	Difference [a.u.]
QED simulation	-380.64662176	-380.64656622	$5.554 \cdot 10^{-5}$
Reference simulation (no QED)	-380.66605850	-380.66601210	$4.640 \cdot 10^{-5}$

## S4 Real-time QED-CC equations

The RT-QED-CC parametrization for the CC states are

$$|\text{QED-CC}\rangle(t) = e^{T(t)} |\text{HF}, 0\rangle e^{i\alpha(t)} \quad (3)$$

$$\langle\Lambda|(t) = \left( \langle\text{HF}, 0| + \sum_{(\mu,n) \neq (\text{HF},0)} \bar{t}_{\mu,n}(t) \langle\mu, n| \right) e^{-T(t)} e^{-i\alpha(t)}. \quad (4)$$

where, for the QED-CCSD-1 model, the (time-dependent) cluster operator reads

$$T(t) = T_e(t) + T_p(t) + T_{int}(t) \quad (5)$$

$$T_e(t) = \sum_{ai} t_{ai}(t) E_{ai} + \frac{1}{2} \sum_{aibj} t_{aibj}(t) E_{ai} E_{bj} \quad (6)$$

$$T_p(t) = \gamma(t) b^\dagger \quad (7)$$

$$T_{int}(t) = \sum_{ai} s_{ai}(t) E_{ai} b^\dagger + \frac{1}{2} \sum_{aibj} s_{aibj}(t) E_{ai} E_{bj} b^\dagger. \quad (8)$$

The time evolution of these states is determined by the time-dependent Schrödinger equation

$$i \frac{d}{dt} |\text{QED-CC}\rangle = H |\text{QED-CC}\rangle \quad (9)$$

$$-i \frac{d}{dt} \langle \Lambda | = \langle \Lambda | H. \quad (10)$$

Notice that the parametrization enforces the normalization of the states at all times

$$\langle \Lambda(t) | \text{QED-CC}(t) \rangle = 1. \quad (11)$$

By projection of these equations onto the space  $S$  spanned by the zero- and one-photon and singly- and doubly-excited Slater determinants

$$S = \text{Span}\{ |\text{HF}, 0\rangle, E_{ai} |\text{HF}, 0\rangle, E_{ai} E_{bj} |\text{HF}, 0\rangle, |\text{HF}, 1\rangle, E_{ai} |\text{HF}, 1\rangle, E_{ai} E_{bj} |\text{HF}, 1\rangle \} \quad (12)$$

we obtain equations for the time derivatives of the amplitudes, the Lagrange multipliers, and the phase factor<sup>4,5</sup>

$$\frac{d\alpha}{dt} = -\langle \text{HF}, 0 | (H + V(t)) e^{T(t)} | \text{HF}, 0 \rangle \quad (13)$$

$$\frac{dt_\mu}{dt} = -i \langle \mu, 0 | e^{-T(t)} (H + V(t)) e^{T(t)} | \text{HF}, 0 \rangle \quad (14)$$

$$\frac{d\gamma}{dt} = -i \langle \text{HF}, n | e^{-T(t)} (H + V(t)) e^{T(t)} | \text{HF}, 0 \rangle \quad (15)$$

$$\frac{ds_\mu}{dt} = -i \langle \mu, n | e^{-T(t)} (H + V(t)) e^{T(t)} | \text{HF}, 0 \rangle, \quad (16)$$

and

$$\frac{d\bar{t}_{\mu,n}}{dt} = i \langle \Lambda | [H + V(t), \tau_{\mu,n}] e^{T(t)} | \text{HF}, 0 \rangle, \quad (17)$$



where  $\tau_{\mu,n}$  is the excitation operator  $\tau_{\mu,n} |\text{HF}, 0\rangle = |\mu, n\rangle$ . In response theory, we would resort to a single Fourier component of the external perturbation

$$V_\omega(t) = \left( V^\omega e^{-i\omega t} + V^{-\omega} e^{i\omega t} \right) e^{\eta t}, \quad (18)$$

Fourier transforms the equations, and derive an effectively time-independent response equation for the Fourier components of the amplitudes and Lagrange multipliers.<sup>4-7</sup> Once the response functions are obtained, the excitation energies are identified with their poles, and the oscillator strength (and other properties) can be obtained from the residues. In the real-time framework, we propagate the equations from a suitable starting point (usually, the QED-CCSD-1 ground state or the QED-HF state) by using the expression of the time derivatives of the amplitudes. To compute the time derivative, it is sufficient to notice that the expressions correspond to time-dependent  $\Omega$  and Jacobian of the QED-CC method.<sup>8,9</sup> A suitable numerical integrator method is thus necessary, such as Runge-Kutta or Euler-Lagrange. The properties in the frequency domain, such as the absorption spectrum, can be obtained from a Fast Fourier Transform of the corresponding time-dependent quantities.<sup>10,11</sup>

## S5 Molecular geometries

In this section, we report the molecular geometries of all the systems studied in the paper.

**Table S7: Molecular geometry of the  $(\text{H}_2)_2$  system. The coordinates are provided in Angstrom  $\text{\AA}$ .**

	Atom	x [ $\text{\AA}$ ]	y [ $\text{\AA}$ ]	z [ $\text{\AA}$ ]
1	H	0.38	0.00	0.00
2	H	-0.38	0.00	0.00
3	H	0.50	50.0	0.00
4	H	0.50	50.76	0.00

**Table S8: Molecular geometry of the  $(\text{H}_2)_2$  system. The coordinates are provided in Angstrom  $\text{\AA}$ .**

	Atom	x [ $\text{\AA}$ ]	y [ $\text{\AA}$ ]	z [ $\text{\AA}$ ]
1	H	0.38	0.00	0.00
2	H	-0.38	0.00	0.00
3	H	0.50	50.0	0.00
4	H	0.50	50.78	0.00

**Table S9: Molecular geometry of the  $(\text{H}_2)_2$  system. The coordinates are provided in Angstrom  $\text{\AA}$ .**

	Atom	x [ $\text{\AA}$ ]	y [ $\text{\AA}$ ]	z [ $\text{\AA}$ ]
1	H	0.38	0.00	0.00
2	H	-0.38	0.00	0.00
3	H	0.50	5.0	0.00
4	H	0.50	5.76	0.00

**Table S10: Molecular geometry of the  $(\text{H}_2)_2$  system. The coordinates are provided in Angstrom  $\text{\AA}$ .**

	Atom	x [ $\text{\AA}$ ]	y [ $\text{\AA}$ ]	z [ $\text{\AA}$ ]
1	H	0.38	0.00	0.00
2	H	-0.38	0.00	0.00
3	H	0.50	5.0	0.00
4	H	0.50	5.76	0.00

**Table S11: Molecular geometry of the succinic semialdehyde  $\text{C}_4\text{H}_6\text{O}_3$ . The coordinates are provided in Angstrom  $\text{\AA}$ .**

	Atom	x [ $\text{\AA}$ ]	y [ $\text{\AA}$ ]	z [ $\text{\AA}$ ]
1	O	0.000000000000	0.000000000000	0.000000000000
2	O	-2.270583565958	0.000000000000	0.000000000000
3	C	-1.212610304804	0.613672647820	0.000000000000
4	C	-1.068159131583	2.120156185050	0.011441617514
5	C	-2.411117455476	2.837430857609	-0.057315304969
6	C	-2.220456659507	4.332212528542	-0.088666176173
7	O	-1.119001321111	4.871278844754	-0.047341313890
8	H	-0.538724127286	2.401902230843	0.929108442623
9	H	-0.449883807544	2.403864608024	-0.848489638121
10	H	-2.961124981613	2.547524594807	-0.958963634409
11	H	-3.029742645520	2.590464855790	0.811921974598
12	H	-3.145829269219	4.929417388464	-0.149259067505
13	H	-0.085208478076	-0.977284779926	-0.002763003539

**Table S12: Water molecular geometry. The coordinates are provided in Angstrom Å.**

	Atom	x [Å]	y [Å]	z [Å]
1	H	0.86681	0.60144	5.00
2	H	- 0.86681	0.60144	5.00
3	O	0.00000	-0.07579	5.00

## References

- (1) Folkestad, S. D.; Kjørnstad, E. F.; Myhre, R. H.; Andersen, J. H.; Balbi, A.; Coriani, S.; Giovannini, T.; Goletto, L.; Haugland, T. S.; Hutcheson, A. et al. e T 1.0: An open source electronic structure program with emphasis on coupled cluster and multilevel methods. *The Journal of Chemical Physics* **2020**, *152*, 184103.
- (2) Huber, C.; Klamroth, T. Explicitly time-dependent coupled cluster singles doubles calculations of laser-driven many-electron dynamics. *The Journal of chemical physics* **2011**, *134*.
- (3) Feit, M.; Fleck Jr, J.; Steiger, A. Solution of the Schrödinger equation by a spectral method. *Journal of Computational Physics* **1982**, *47*, 412–433.
- (4) Koch, H.; Jorgensen, P. Coupled cluster response functions. *The Journal of chemical physics* **1990**, *93*, 3333–3344.
- (5) Pedersen, T. B.; Koch, H. Coupled cluster response functions revisited. *The Journal of chemical physics* **1997**, *106*, 8059–8072.
- (6) Castagnola, M.; Riso, R. R.; Barlini, A.; Ronca, E.; Koch, H. Polaritonic response theory for exact and approximate wave functions. *Wiley Interdisciplinary Reviews: Computational Molecular Science* **2024**, *14*, e1684.
- (7) Olsen, J.; Jørgensen, P. Linear and nonlinear response functions for an exact state and for an MCSCF state. *The Journal of chemical physics* **1985**, *82*, 3235–3264.
- (8) Helgaker, T.; Jorgensen, P.; Olsen, J. *Molecular electronic-structure theory*; John Wiley & Sons, 2013.
- (9) Haugland, T. S.; Ronca, E.; Kjørnstad, E. F.; Rubio, A.; Koch, H. Coupled cluster theory for molecular polaritons: Changing ground and excited states. *Physical Review X* **2020**, *10*, 041043.

- (10) Skeidsvoll, A. S.; Balbi, A.; Koch, H. Time-dependent coupled-cluster theory for ultrafast transient-absorption spectroscopy. *Physical Review A* **2020**, *102*, 023115.
- (11) Skeidsvoll, A. S.; Moitra, T.; Balbi, A.; Paul, A. C.; Coriani, S.; Koch, H. Simulating weak-field attosecond processes with a Lanczos reduced basis approach to time-dependent equation-of-motion coupled-cluster theory. *Physical Review A* **2022**, *105*, 023103.